Skyrme-Hartree-Fock-BCS approach to ^{229m}Th and neighboring nuclei

Nikolay Minkov, ^{1,*} Adriana Pálffy, ^{2,†} Philippe Quentin, ^{3,‡} and Ludovic Bonneau^{3,§}

¹Institute for Nuclear Research and Nuclear Energy,

Bulgarian Academy of Sciences, Tzarigrad Road 72, BG-1784 Sofia, Bulgaria

²University of Würzburg, Institute of Theoretical Physics and Astrophysics, Am Hubland, 97074 Würzburg, Germany

³LP2i Bordeaux, UMR 5797, Université de Bordeaux, CNRS, F-33170, Gradignan, France

(Dated: August 21, 2024)

The microscopic origin of the 229m Th isomer and its possible manifestation also in neighboring nuclei is explored within a selfconsistent Skyrme Hartree-Fock plus Bardeen-Cooper-Schrieffer approach. By using the well established SIII Skyrme parametrization, without any special adjustments related to low-energy isomer, the single-particle spectrum provided by the model reproduces the correct isomer $K^{\pi}=3/2^+$ spin and parity, and the relative proximity of the isomeric state to the $K^{\pi}=5/2^+$ ground state, yet on the keV scale. We show that this approach may provide microscopic estimates for some related observables, such as the quadrupole and octupole moments, deformation parameters as well as magnetic dipole moments. Its ability to provide a prediction for the M1 isomer transition probability is discussed. The obtained 229 Th single-particle structure is compared with that provided by calculations in neighbouring actinide isotopes and isotones, allowing us to assess the more general role of the considered mechanism for the formation of low-energy isomers.

I. INTRODUCTION

A unique nuclear isomer with energy of only 8 eV has become recently the subject of intense investigation in atomic, nuclear and laser physics and metrology. The 229m Th isomer is so far an exceptional case of nuclear excitation optically accessible by suitable laser sources in the vacuum-ultraviolet (VUV). This promises a new frequency standard [1–3], and means to probe the variation of fundamental constants [4–6] or search for light dark matter [6, 7] in unprecedented ways. ²²⁹Th has a ground state (GS) spin and parity $5/2^+$, an isomeric state (IS) spin and parity $3/2^+$ and the transition between the two states represents a magnetic dipole M1and electric quadrupole E2 mixture. The experimental determination of the transition energy has come a long way in the past decades [8–14], involving observation of both the internal conversion [15, 16] and the radiative decay channels [13, 14, 17]. The breakthrough for the design of the nuclear clock occurred this very year (2024), with three reported experiments which succeeded in direct laser driving of the isomeric transition in Th-doped VUV transparent crystals [14, 17, 18]. The experimental accuracy for the nuclear transition frequency increased from GHz [14, 17] to kHz in the most recent experiment using a VUV frequency comb [18].

From nuclear structure perspective, early theoretical estimates for the isomer reduced transition probability B(M1) and the isomer magnetic moment $\mu_{\rm IS}$ were made in Refs. [19, 20] using the Alaga branching ratios [21] and

the Nilsson model [22]. Alternative predictions for the B(M1) and B(E2) reduced transition probabilities for the $3/2^+ \rightarrow 5/2^+$ isomer transition have been made in Refs. [23, 24] using the quasiparticle-plus-phonon model [25] in an overall description of the ²²⁹Th spectrum without particular consideration of the isomer properties. Furthermore, microscopic calculations involving the $3/2^+$ isomer energy have been performed within the Relativistic Mean Field (RMF) theory [26, 27] and the Hartree-Fock-Bogoliubov (HFB) approach [28] as a part of the efforts to determine the isomer decay rate sensitivity to possible temporal variations of the fine structure constant α , without particular focus on the origin and formation mechanism of the isomer.

The 229m Th isomer formation mechanism was recently described within a model approach providing an explanation for the appearance of the extremely low-energy state as the effect of a very fine interplay between collective quadrupole-octupole degrees of freedom and the singleparticle (s.p.) motion of the odd neutron in ²²⁹Th [29– 31]. The IS was considered as the bandhead of a quasiparity-doublet spectrum built on a $K^{\pi} = 3/2^+$ quasiparticle (q.p.) excitation (3/2[631] s.p. orbital) which is coupled via Coriolis mixing to the $K^{\pi} = 5/2^{+}$ (5/2[633] orbital) GS. Here, K and π refer to the projection of the total nuclear angular momentum \hat{I} on the body-fixed principal symmetry axis and the parity, respectively, while the notation $K[Nn_z\Lambda]$ involves the usual asymptotic Nilsson quantum numbers [32], explained in more detail below. The approach combines the features of a collective (coherent) quadrupole-octupole model (CQOM) [33–37] and deformed shell model (DSM) [38] with pairing correlations of Bardeen-Cooper-Schrieffer (BCS) type. The overall CQOM-DSM model approach provides theoretical predictions for the B(M1) and B(E2) isomer decay rates [29] and GS and IS magnetic moments [30] in ²²⁹Th. Also, it allows one to make a detailed assess-

^{*}Electronic address: nminkov@inrne.bas.bg

[†]Electronic address: adriana.palffy-buss@uni-wuerzburg.de

[‡]Electronic address: quentin@cenbg.in2p3.fr §Electronic address: bonneau@lp2ib.in2p3.fr

ment of the shape-deformation and intrinsic-motion conditions, including the quasi-degeneracy of the two s.p. orbitals, which determine the isomer-formation mechanism and the resulting energy and electromagnetic properties of the metastable state [31].

The relevance of the CQOM-DSM approach in the explanation of key 229m Th properties raises the question about the validity of the proposed isomer-formation mechanism on the deeper microscopic mean-field level. It is therefore important to understand how the deformation and intrinsic effective interactions determine the isomer-formation conditions in the solution of the manybody problem for ²²⁹Th. More specifically, it is interesting to examine how deformations and effective interactions govern the intrinsic states which could be responsible for the isomer excitation, the related energy-levels proximity or quasi-degeneracy, the overall energy and electromagnetic characteristics of the nucleus. The same question naturally extends to other nuclei in the same mass region requiring to check how the isomer-formation conditions evolve with the changing intrinsic structure.

The purpose of this work is to clarify the above questions within the framework of the Skyrme energy-density functional (EDF) approach, including BCS pairing correlations with selfconsistent blocking. To solve this task we employ a Hartree-Fock-BCS (HFBCS) approximation with time-odd terms and seniority pairing correlations as formulated in Ref. [39]. As a basic Skyrme EDF option we take the SIII Skyrme parametrization [40]. The timeodd terms, taken in a "minimal" scheme with spin and current vector fields, as defined in Ref. [39] and recalled here in Appendix A for self-consistency, allow one to take into account the polarization effect of the unpaired nucleon on the even-even core resulting in time-reversal symmetry breaking, and hence a suppression of Kramers degeneracy. The algorithm is elaborated for calculations without imposed reflection symmetry, still keeping the axial symmetry, which allows for possible solutions with non-zero "pear-shape" octupole deformation. The selfconsistent equations are solved by diagonalization of the Hartree–Fock (HF) Hamiltonian in an axially-symmetric deformed harmonic oscillator basis [41]. The approach is especially suitable for nuclei in the actinide mass region known to exhibit axial quadrupole or axial quadrupoleoctupole deformations.

Some basic explanations of the approach and its application for description of magnetic moments and spingyromagnetic quenching in odd-mass nuclei have been
presented in Ref. [39]. In Refs. [42–45] the model was
applied to K-isomeric excitations in heavy even-even nuclei. Its capability to handle octupole deformation was
demonstrated in Ref. [42]. All these HFBCS applications
with the SIII force show that the approach allows a reasonably good description of the spectroscopic properties
of interest. We remark that, owing to the BCS treatment of pairing and the Slater approximation used for
the exchange Coulomb terms, the present study is expected to share similarities with the HFB calculations of

Ref. [28], but brings new insights because of the breaking of time-reversal symmetry in the one-quasiparticle intrinsic states inherent to selfconsistent blocking. The other essential feature of the present study is the consideration of the reflection-asymmetric (octupole) deformation, missing in the result of Ref. [28], which turns out to play a crucial role in the understanding of the 229m Th isomer properties.

It should be noted here that presently there is a large variety of nuclear EDF approaches with developed highperformance computer codes which can be applied to the 229m Th problem. For instance, we refer here to the HFODD solver for the HF and HFB problem in Cartesian deformed harmonic-oscillator basis [46], the Skyrme HFBCS Ev8 [47] and HFB Skv3D [48] codes realized in three-dimensional coordinate space and many others (see also further references in these articles). All these state-of-the-art approaches can provide an advanced symmetry-unrestricted treatment of 229m Th with high-computation efficiency and numerical accuracy, use of a large variety of effective interactions, and many other features. At the same time, we consider that the present Skyrme HFBCS approach, with the extensively tested SIII interaction, is capable to provide a relatively simple and easily understandable solution. It adequately incorporates the key features of an odd-mass nucleus with core polarization, pairing correlations, axial quadrupoleoctupole deformation and the resulting energy and electromagnetic properties.

We apply the Skyrme HFBCS approach with the characteristics described above to the particular study of the ²²⁹Th ground-state and the lowest q.p. excitations, trying to infer the possible formation mechanism of the $3/2^+$ isomer and its spectroscopic properties. It is clear that the accuracy level of the nuclear self-consistent approach is far away from the eV precision needed to reproduce the measured isomer energy. Nevertheless, the thorough examination of the ^{229m}Th HFBCS solution under different model conditions is of an utmost importance to understand the microscopic origin of the isomer-formation mechanism and to follow its possible evolution in other nuclei as well. Such a study requires a fine evaluation of some basic conditions, including the core polarization induced by the unpaired neutron, the pairing correlations and the effect of reflection-asymmetric (octupole) shape, in much deeper details than usually considered in the global application of the standard many-body approaches. To this end we have structured our study in separate steps allowing us to assess the effect of adding the single nucleon to the even-even core and imposing or not reflection symmetry, on the formation of low energy q.p. excitations including the extremely low-lying isomer state.

Our step-wise procedure goes as follows. We start with the solution for the even-even core nucleus 228 Th for which the s.p. orbitals around the Fermi level are analysed both in the reflection-symmetric and octupole cases, with a focus on the relative position of the $3/2^+$

and $5/2^+$ orbitals. This allows us to gain a deeper understanding of the structure changes occurring after the unpaired neutron is added in ²²⁹Th. (In principle, one can equally well consider ²³⁰Th as a core nucleus from which a neutron is removed.) We then proceed with the HFBCS iterative process with selfconsistent blocking using the same pairing constants and basis parameters of the GS solutions of the core, and find the corresponding ²²⁹Th solutions, with and without reflection symmetry, for the $5/2^+$, $3/2^+$ and a few other neighboring q.p. excitations. This allows us to assess the ability of the HFBCS algorithm to handle the proximity of the $3/2^+$ excitation to the $5/2^+$ GS under the different shape conditions. For each state we obtain model predictions for a number of structure quantities—deformations, electric and magnetic moments and gyromagnetic factors, with some of them being compared with values obtained in the CQOM-DSM approach. We note that the magnetic dipole moments are of special importance since their values incorporate the underlying electromagnetic characteristics of the considered states and in particular the 229m Th isomer decay properties.

The calculations are extended to the neighboring ²²⁷Th and ²³¹Th isotopes and ²²⁷Ra and ²³¹U isotones, taking ²²⁶Th, ²³⁰Th and ²²⁶Ra, ²³⁰U, respectively, as initial even-even cores for the calculation. This allows us to examine the "migration" of the ²²⁹mTh isomer-forming s.p. orbitals and their close neighbors in the vicinity of ²²⁹Th. The results outline quite a detailed picture for the evolution of the intrinsic conditions which may govern the emergence of low-energy metastable states in the considered actinide mass region.

The paper is structured as follows. In Sec. II we apply the HFBCS approach to the core nucleus ²²⁸Th. Subsequently, in Sec. III the elaborated prescription is applied to ²²⁹Th for the two cases of reflection-symmetry and octupole deformation. The results are analysed and we discuss the capability of the used effective interactions (both in the particle-hole and particle-particle/hole-hole channels) to provide conditions appropriate for isomer formation. We extend our study to the neighboring nuclei in Sec. IV outlining the evolution of the overall low-energy excitation conditions around ²²⁹Th. The paper concludes in Sec. V with a discussion and remarks on further perspectives of our approach for the study of ^{229m}Th and similar phenomena in other nuclei.

II. HFBCS APPROACH TO THE THORIUM PROBLEM. THE ²²⁸TH CORE.

A. HFBCS solution with and without reflection symmetry

The HFBCS algorithm applied with reflection symmetry provides a solution with axial quadrupole deformation. The basis is symmetrized with respect to the z-axis origin and the variation procedure starts with an initial

Woods-Saxon potential with deformation defined by the quadrupole parameter $\beta_2 = 0.2$. The converged result includes the obtained quadrupole moment and, for the odd mass nucleus, the magnetic dipole moment and gyromagnetic factor. In this case the intrinsic parity is conserved and the s.p. wave functions possess a definite parity.

When the reflection symmetry is no longer imposed, one is often confronted with convergence difficulties because of shifts in the center-of-mass position on the symmetry axis during the iteration procedure. This requires a specific center-of-mass constraint to fix its position at the origin of the intrinsic frame. In addition, to allow the HFBCS algorithm to find a potential octupole solution, we start the calculation with an initial mean field generated by a Wood-Saxon potential with the octupole deformation parameter value of $\beta_3 = 0.1$ in addition to the quadrupole $\beta_2 = 0.2$ deformation. We consider that the model indicates the presence of octupole shape if the solution is obtained with non-zero octupole moment and β_3 deformation and the resulting total energy is lower compared to that in the reflection-symmetric (pure quadrupole) solution. This solution corresponds to axial quadrupole-octupole deformation, while the s.p. wave functions appear with mixed parity and can be only characterized by the average (expectation) value $\langle \pi \rangle$ of the parity operator calculated in the given state.

B. Axially-deformed harmonic oscillator basis

The single-particle HF Hamiltonian is diagonalized in the axially-deformed harmonic oscillator (ADHO) basis [41]. This basis is characterized by the oscillator frequencies along the symmetry axis (chosen to be the z axis), ω_z , and in a direction perpendicular to the z axis, ω_\perp . These two frequencies define ω_0 as an equivalent (volume conserving) frequency by $\omega_0^3 = \omega_z \omega_\perp^2$. The ADHO basis is conveniently referred to through the spherical equivalent oscillator constant $b = \sqrt{m\omega_0/\hbar}$, where m is the mean nucleon mass, and the deformation parameter $q = \omega_\perp/\omega_z$.

In practice the ADHO basis is truncated as explained in Ref. [49]. The basis states are eigenvectors of the axially-deformed, two-dimensional harmonic-oscillator Hamiltonian and carry the Nilsson quantum numbers $|Nn_z\Lambda\Sigma\rangle$ where n_z denotes the phonon number along the symmetry axis, $N=n_z+n_\perp$ is the total phonon number, with n_\perp the phonon number in a direction perpendicular to the symmetry axis, Λ and Σ are the projections on the symmetry axis of the orbital and spin angular momenta, respectively. One has $K=\Lambda+\Sigma$. The states $|Nn_z\Lambda\Sigma\rangle$ retained in the truncated basis satisfy the condition $\omega_z(n_z+1/2)+\omega_\perp(n_\perp+1)\leqslant\omega_0(N_0+3/2),$ where the basis truncation parameter N_0 is such that N_0+1 represents the number of retained spherical shells when q=0 and takes here the value $N_0=16$.

Because of the finiteness of the s.p. basis, we have to optimize the b and q parameters by minimizing the

total energy for the ground-state solution (including the pairing energy). For the 228 Th core nucleus we find b = 0.480 and q = 1.20.

Finally, all numerical integrations, in particular to compute the matrix elements of the Hartree-Fock Hamiltonian, are performed by Gauss-Hermite (over the z coordinate) and Gauss-Laguerre (over the radial coordinate) quadratures with 30 and 15 points, respectively.

C. Determination of the BCS pairing strengths

In our approximate treatment, we define different constant neutron and proton averaged matrix elements determining the strength of the BCS pairing correlations up to 6 MeV above the chemical potentials with a smoothing factor defined by a width of 0.2 MeV (see Ref. [50] for details). For a charge state $\tau=n,p$ (n-neutrons, p-protons), their dependence on the corresponding fermion numbers N_{τ} is parametrized as $V_{\tau}=-G_{\tau}/(11+N_{\tau})$ (see Ref. [51]). In a recent paper [52] some of the present authors have shown that in well deformed nuclei, the determination of the two strength parameters (G_n,G_p) above can be almost equivalently performed either by fitting three-point odd-even mass differences $\Delta^{(3)}$ (around odd nuclei) or the energy of the first 2_1^+ level in even-even nuclei. In the latter case the 2_1^+ energy is related to the calculated moment of inertia \mathfrak{J} within the simple quantal rotor approximation $E(2_1^+)=\frac{\hbar^2}{2\mathfrak{J}}[2(2+1)]=3\hbar^2/\mathfrak{J}$.

In view of the easier numerical task associated with computing \mathfrak{J} with respect to $\Delta^{(3)}$, we chose to perform our fit within the second approach. We note that the moments of inertia of even-even nuclei are calculated within the usual Inglis-Belyaev approach [53–55] supplemented by so-called self-consistent Thouless-Valatin corrections [56]. The enhancement coefficient (in practice a 1.32 multiplication factor) to take care of these corrections has been taken from Ref. [57] where it has been determined upon using the D1S Gogny interaction and found in many instances (see, e.g., [44]) to be valid also for selfconsistent solutions using the SIII interaction. It is thus clear that our calculated moments of inertia depend on three important approximations (pure rotor dynamics, adiabaticity and approximate Thouless-Valatin corrections).

Keeping the above in mind, upon fitting the pairing strengths on the experimental $E(2_1^+)$ value of 57.8 keV [58] for the ²²⁸Th ground state solution we obtain $G_n = 16.0$ MeV and $G_p = 14.4$ MeV corresponding to a theoretical energy value of $E^* = 58.4$ keV. These values for the pairing strength parameters are close to the results of a systematic fit in Ref. [44] which yielded $G_n = 15.80$ MeV and $G_p = 14.23$ MeV.

D. Exploring the ²²⁸Th core

We have performed HFBCS calculations for the 228 Th core using the parameters discussed above with and without imposed reflection symmetry. The results are given in Table I. They include the theoretical total energy and 2_1^+ excitation energy approximated by $E_{\rm th}^*(2_1^+) = 3\hbar^2/\mathfrak{J}_{th}$, as well as other characteristics of the solutions, namely neutron and proton pairing gaps Δ_n and Δ_p , mass and charge quadrupole moments Q_{20}^m and Q_{20}^p , respectively, and the corresponding quadrupole deformation parameters β_2^m and β_2^p . In addition, the mass octupole moment Q_{30}^m and octupole deformation β_3^m are given for the reflection-unconstrained (asymmetric) solution. The relevant definitions and relations connecting the quadrupole and octupole moments calculated in the code and the correspondingly deduced deformation parameters are given in Appendix B.

The following comments can be made upon investigating the results given in Table I:

- (i) The pairing strengths fitted in the reflection symmetric solution lead to an underestimation of the experimental 2_1^+ excitation energy in the reflection-unconstrained calculation. The last line of Table I shows the results obtained after a re-adjustment of the pairing strengths to more closely match the theoretical value to the experimental one $E(2_1^+)=57.8~{\rm keV}$, which yields $G_n=16.5~{\rm MeV}$ and $G_p=14.9~{\rm MeV}$ (keeping a constant ratio $G_p/G_n=0.9$).
- (ii) In the reflection-asymmetric solution the total energy is by 0.5 MeV lower than that in the reflection-symmetric solution for the initial pairing strengths $G_n=16.0$ MeV and $G_p=14.4$ MeV. The former solution is characterized by a non-zero octupole moment Q_{30}^m and the corresponding octupole deformation parameter is about $\beta_3^m=0.12-0.13$. This result is in agreement with earlier calculations of 228 Th ground-state properties within the self-consistent relativistic Hartree-Bogoliubov model of Ref. [59].

Having obtained the solutions in Table I, we can analyze the s.p. spectrum of the core nucleus ²²⁸Th in its ground state. More precisely, we inspect the positions of the neutron orbitals near the Fermi level. Because of the good-rotor character of the ²²⁸Th nucleus and its neighbors, we may expect that the positions of the $5/2^+$ and $3/2^+$ orbitals carry information about the formation of the ground and isomeric states in the neighboring odd-mass nucleus ²²⁹Th after a neutron is added to the core. In Fig. 1 the s.p. levels of ²²⁸Th obtained in the reflection-symmetric case with the pairing strengths $G_n = 16.0 \text{ MeV}$ and $G_p = 14.4 \text{ MeV}$ are displayed. On the MeV energy scale of the figure, the two orbitals $5/2^+$ and $3/2^+$ are found to be virtually degenerate. The 3/2⁺ orbital stays on the Fermi level at neutron number N=138, while the $5/2^+$ orbital is located only 11 keV above it. In addition, in Fig. 1 we see a $5/2^-$ orbital appearing 60 keV above the $3/2^+$ and $5/2^+$ orbitals. Its presence could be related with the appearance of oc-

TABLE I: Total energy $(E_{\rm tot})$, first 2_1^+ excitation energy approximated by $E_{\rm th}^*(2_1^+) = 3\hbar^2/\mathfrak{J}_{th}$, neutron (Δ_n) and proton (Δ_p) pairing gaps, mass and charge quadrupole moments $(Q_{20}^m$ and $Q_{20}^p)$, and quadrupole deformations $(\beta_2^m$ and $\beta_2^p)$, mass octupole moment (Q_{30}^m) and octupole deformation (β_3^m) obtained for the ground state of 228 Th in the reflection-symmetric and reflection-unconstrained HFBCS solutions with different sets of pairing strengths G_n and G_p (see text for further explanations).

G_n (MeV)	G_p (MeV)	E_{tot} (MeV)	$E_{\rm th}^*(2_1^+)$ (keV)	Δ_n (MeV)	Δ_p (MeV)	Q_{20}^m (fm ²)	β_2^m	Q_{20}^p (fm ²)	β_2^p	$Q_{30}^m \atop (b^{3/2})$	β_3^m
			Re	effection-	-symmet	ric solutio	n				
16.0	14.4	-1737.900	58.4	0.867	0.888	2057.042	0.210	818.514	0.212	_	-
			Re	flection-	asymme	tric solutio	on				
16.0	14.4	-1738.4118	49.3	0.826	0.765	1967.5	0.200	783.085	0.202	2.792	0.130
16.5	14.9	-1738.7811	58.0	0.952	0.879	1954.1	0.199	777.504	0.201	2.659	0.124

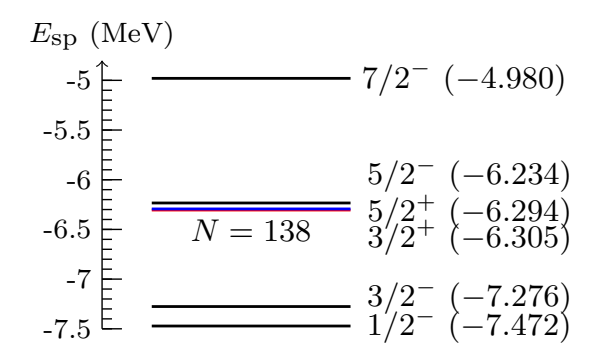


FIG. 1: Neutron single-particle levels near the Fermi level of 228 Th obtained in reflection-symmetric Skyrme-SIII HFBCS calculation with $G_n=16.0$ MeV and $G_p=14.4$ MeV. Each level denoted by K^{π} is Kramers degenerate and its energy (in MeV) is given in brackets. The lines depicting the $3/2^+$ and $5/2^+$ orbitals, drawn in red and blue, respectively, are degenerate and thus indistinguishable in the given scale. Among them, the lower lying $3/2^+$ orbital is the Fermi level.

tupole deformation in the ground-state shape of 228 Th and may play a role in forming the structure of the 229 Th spectrum related to octupole deformation. We also notice the other neighboring orbitals, $7/2^-$ above and $3/2^-$ and $1/2^-$ below the Fermi level, which, in addition, may play a role in the formation of s.p. excitations in the nuclei around 228 Th. It is interesting to remark that the same orbitals are identified in the DSM calculations for 229 Th performed in the space of quadrupole β_2 and octupole β_3 deformations (see Fig. 1 in Ref. [31]). It is suggested there that all these orbitals may cross each other in certain deformation ranges and, therefore, it can be expected that their interaction will influence the related structure properties of the nuclei in the region of 229 Th.

The s.p. spectra associated with orbitals from the reflection-asymmetric solutions of Table I, i.e., the case with octupole deformation, are shown in Fig. 2. The notation $\langle + \rangle$ ($\langle - \rangle$) in the s.p. labels denotes a positive

(negative) expectation value of the parity operator. We notice that the $3/2^{\langle + \rangle}$ orbital now appears about 360 keV above the $5/2^{\langle + \rangle}$ level. This energy difference is significantly larger than the corresponding energy difference of 11 keV in the reflection-symmetric case presented in Fig. 1. Also, the $5/2^{\langle - \rangle}$ orbital now appears considerably lower in energy than the $5/2^-$ level.

To understand this behaviour, it is worth recalling that the reflection asymmetric shape of the ground state of ²²⁸Th shows us that the intrinsic parity breaking in the HFBCS solution for this nucleus is energetically favorable. This is manifested by parity mixing in the s.p. states, which is according to Refs. [60, 61] especially large in pairs of states whose dominant Nilsson configurations are of the form $K^{\pi}[Nn_z\Lambda]$ and $K^{-\pi}[N'n_z'\Lambda]$ where |N'-N|=1, 3 and $|n'_z-n_z|=1$, 3, with $\pi=(-1)^N$. These selection rules are associated with the octupoledeformed central mean field, which is dominant as compared to the spin-orbit field. For example in the solution obtained with $G_n = 16.0$ MeV and $G_p = 14.4$ MeV, we have $\langle \frac{5}{2} \langle + \rangle | \pi | \frac{5}{2} \langle + \rangle \rangle = 0.433$ and $\langle \frac{3}{2} \langle + \rangle | \pi | \frac{3}{2} \langle + \rangle \rangle = 0.241$. In the former case, the largest two Nilsson contributions to the $5/2^{(+)}$ state are $5/2^{+}[633]$ and $5/2^{+}[642]$, whereas the largest two Nilsson components of the $5/2^{\langle - \rangle}$ are $5/2^-[752]$ and $5/2^-[743]$. The octupole coupling between these two 5/2 states involves a leading component in one state and a subleading component in the other state. This occurs in two distinct ways, leading to a parity mixing. On the other hand, the dominant Nilsson configuration of the $3/2^{(+)}$ state is $3/2^{+}[651]$ whereas a $3/2^{\langle -\rangle}$ state is found just below -7.5 MeV (outside the range plotted in Fig. 2) with a dominant configuration $3/2^{-}[741]$. The resulting parity mixing between these two 3/2 states thus occurs essentially through the coupling of these leading Nilsson configurations.

Moreover, the effect of this octupole coupling on the single-particle energies generally preserves the ordering of the states characterized by their average parity, as expected from a reasoning based on second-order perturbation theory. This is typically the case in the pair

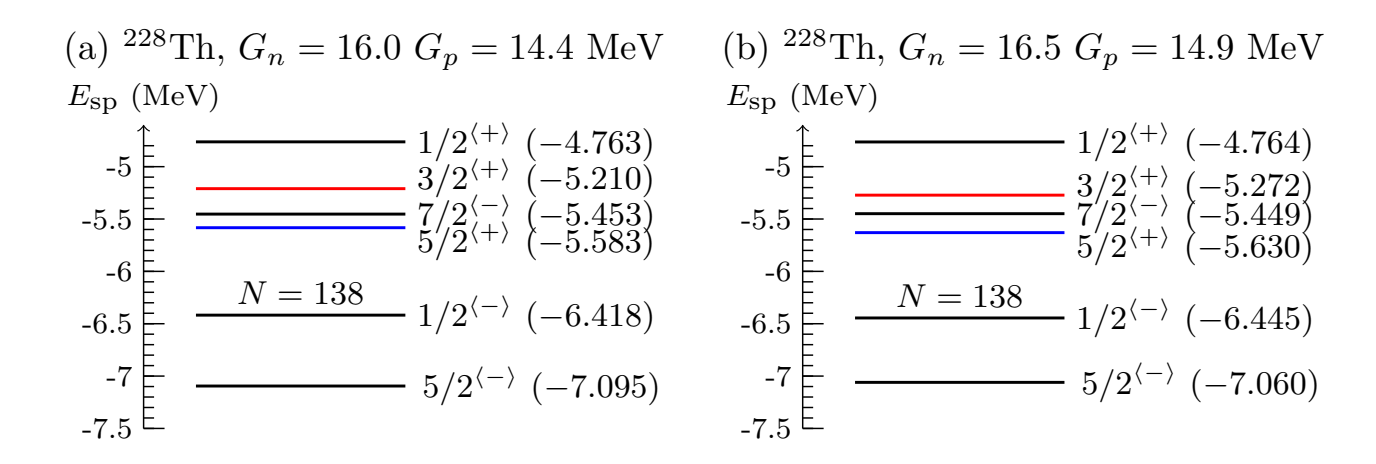


FIG. 2: Neutron single-particle levels near the Fermi level of 228 Th obtained in reflection-unconstrained Skyrme-SIII HFBCS calculation with (a) $G_n=16.0$, $G_p=14.4$ MeV and (b) $G_n=16.5$, $G_p=14.9$ MeV. Each level denoted by $K^{\langle \pi \rangle}$ is Kramers degenerate and its energy (in MeV) is given in parenthesis. The notations $\langle \pm \rangle$ correspond to the sign of the average parity $\langle \pi \rangle$. The lines depicting the $3/2^+$ and $5/2^+$ orbitals are drawn in red and blue, respectively.

of 3/2 states discussed above. Because the coupling between them is strong, the single-particle energy of the $3/2^{\langle + \rangle}$ state significantly increases while that of the $3/2^{\langle - \rangle}$ drops. However, the $5/2^{\langle - \rangle}$ state, expected to lie above the Fermi level and above the $5/2^{\langle + \rangle}$ state for very small octupole moments, happens to drop far below the Fermi level for the actual octupole deformation. At the same time the $3/2^{\langle + \rangle}$ state gets pushed above the $5/2^{\langle + \rangle}$ state, both lying above the Fermi level. By a similar mechanism a $7/2^{\langle - \rangle}$ state is pushed down from far above the Fermi level in the symmetric solution, in such a way that it lies between the $5/2^{\langle + \rangle}$ and $3/2^{\langle + \rangle}$ states just above the Fermi level.

This overall structure of the s.p. spectrum in 228 Th suggests that the $5/2^+$ and $3/2^+$ states may be expected to lie close to each other in the odd-mass nucleus 229 Th. When octupole deformations are taken into account (for the reflection-asymmetric solution), in addition also the $7/2^-$ state is expected to be present in the same vicinity. Comparing Figs. 1 and 2 we remark that the spacing and order of the s.p. levels are more strongly affected by the inclusion of octupole deformation rather than by the fine (re)adjustment of the pairing strengths G_n and G_p .

III. 229TH CALCULATION

A. Calculations of one-quasiparticle states with self-consistent blocking

We perform the HFBCS calculations for 229 Th by separately blocking the orbitals near the 228 Th Fermi level in accordance to the level structures in Figs. 1 and 2. These are the $5/2^+$, $3/2^+$, $5/2^-$ and $7/2^-$ orbitals. The numerical calculations are performed in a regime of broken time-reversal invariance (see Appendix A for the time-

odd terms used) with removed Kramers degeneracy so that each s.p. orbital splits into a pair of positive and negative K counterparts (see Ref. [39] for more details).

Blocking a single-particle state with a positive K quantum number or its pairing partner with the opposite value of the K quantum number leads to time-reversed solutions with the same expectation values of time-even operators, including the total energy. Therefore one can consider only one-quasiparticle states with positive K values in the blocking procedure.

The excitation energies (q.p. bandheads) are determined as

$$E^*(K^{\pi}) = E_{\text{tot}}(K^{\pi}) - E_{\text{tot}}(K^{\pi}_{GS})$$
, (1)

where $E_{\text{tot}}(K_{\text{GS}}^{\pi})$ is the lowest total energy corresponding to the GS orbital.

The calculations were made in the cases of imposed and released reflection symmetry. Calculations with selfconsistent blocking and intrinsic parity breaking are very scarce in the literature [62]. Their convergence is made particularly difficult when two single-particle states with the same K quantum number but opposite parity content are both close to the chemical potential. This precisely happens in the case of the 5/2 one-quasiparticle states of the ²²⁹Th nucleus. In the same spirit as explained in Ref. [63] about selfconsistent blocking in Cranked Hartree-Bogoliubov + Lipkin-Nogami calculations, several "fingerprints" have to be used to identify the state to be blocked. In the present work we use the average parity $\langle \pi \rangle$ in addition to the K quantum number. Even though $\langle \pi \rangle$ turns out to be almost vanishing in some cases, it proves to be efficient to make the blocked calculations converge in the course of Hartree–Fock iterations.

TABLE II: Total energy, $E_{\text{tot}}(K^{\pi})$, excitation energies, $E^*(K^{\pi})$, Eq. (1), neutron (Δ_n) and proton (Δ_p) pairing gaps, mass and charge quadrupole moments (Q_{20}^m) and Q_{20}^p and corresponding deformation parameters β_2^m and β_2^p , magnetic moment (μ) , collective gyromagnetic factor g_R and spin-gyromagnetic quenching q_s obtained by reflection symmetric SIII-HFBCS calculations for blocked $5/2^+$, $3/2^+$, $5/2^-$ and $7/2^-$ orbitals in 229 Th with the set of pairing strengths $G_n = 16.0$ MeV and $G_p = 14.4$ MeV. For each orbital the Nilsson quantum numbers of the leading component and its contribution in the s.p. wave function (in %) is given (see text for further details).

K^{π}	$[Nn_z\Lambda](\%)$	$E_{ m tot}$	E^*	Δ_n	Δ_p	Q_{20}^{m}	β_2^m	Q_{20}^{p}	β_2^p	μ	g_R	q_s
		(MeV)	(keV)	(MeV)	(MeV)	(fm^2)		(fm^2)		(μ_N)		
$\frac{5}{2}$ +	[633] (56.4)	-1743.3668	0.0	0.642	0.882	2150.9	0.217	850.6	0.219	0.7366	0.291	0.738
$\frac{3}{2}$ +	[631] (31.9)	-1743.3497	17.1	0.645	0.884	2147.9	0.217	849.5	0.219	-0.3128	0.352	0.765
$\frac{5}{2}$	[752] (35.3)	-1743.3499	16.9	0.644	0.884	2144.9	0.217	848.3	0.219	-0.2457	0.473	0.714
$\frac{7}{2}$	[743] (52.1)	-1742.4774	889.4	0.774	0.904	2135.0	0.216	843.2	0.217	-0.4659	0.368	0.735

B. Numerical results

The obtained numerical results of the reflection-symmetric and asymmetric calculations are given in Tables II and III, respectively. The corresponding one-neutron q.p. excitation (bandhead) energy levels are illustrated in Fig. 3. In both cases the obtained $5/2^+$ state has the lowest energy and thus correctly represents the experimentally observed 229 Th ground state.

Our results for the reflection symmetric case are presented in Table II and Fig. 3(a). Summarizing our findings, we note that:

- (i) The $E^*(3/2^+)$ excitation energy corresponding to the 229m Th isomer appears at 17.1 keV. Although it is 3 orders of magnitude larger than the experimental isomer energy of 8 eV, from nuclear structure point of view the model $3/2^+$ state appears almost degenerate with the $5/2^+$ ground state. Note that the SIII effective interaction used reproduces the Nilsson quantum numbers of the leading components in the s.p. wave function of the two orbitals 5/2[633] and 3/2[631] (see Table II) widely adopted in the literature and experimental data bases [58].
- (ii) Regarding the other two considered orbitals, we see that while the $E^*(7/2^-)$ energy is about 0.9 MeV, obviously out of the range of very low-energy excitations, the energy of the $5/2^-$ state is almost degenerate with and slightly below the $3/2^+$ isomer. From the model point of view this can be understood by the almost degenerate $5/2^+$ and $5/2^-$ orbitals observed in Fig. 1 for 228 Th. On the other hand the obtained $5/2^-$ q.p. excitation in 229 Th can be associated with the 5/2[752] bandhead, identified in the experiment with energy of about 143 keV [58]. The latter is considered as the negative-parity counterpart of the 5/2[633] ground state within the yrast quasi-parity-doublet of ²²⁹Th. Here the energy of this level is essentially underestimated, but as shown later on, this result considerably changes with the inclusion of the octupole deformation.
 - (iii) The calculations also provide predictions for the

quadrupole moments and deformation, the magnetic dipole moments μ , the collective gyromagnetic factor of the even-even core g_R and the spin-gyromagnetic quenching q_s in the four considered q.p. states of ²²⁹Th. Details on the calculation of the magnetic moments and gyromagnetic factors with the quenching effect are given in Secs. IIC, IIID and Appendix B of Ref. [39]. From Table II we see that, similarly to the DSM-CQOM calculations [30, 31], the obtained GS magnetic moment of about $0.74\mu_N$ overestimates the experimental values of $0.360(7)\mu_N$ [64] and $\mu_{\rm GS} = 0.45(4)\mu_N$ [65]. On the other hand, again similarly to DSM-CQOM, the obtained IS magnetic moment of $-0.31~\mu_N$ agrees well with the recent experimental value of $-0.37(6)\mu_N$ [66, 67].

We note that the present HFBCS calculations provide different collective and spin gyromagnetic factors for the different blocked orbitals. The collective gyromagnetic factor g_R is calculated for the polarized even-even core in the cranking approximation with BCS pairing excluding the blocked state and its conjugate state (for the definition of the latter see Sec. IIA of Ref. [39]). On the other hand the DSM-CQOM calculations [30, 31] use common gyromagnetic factors for the ground and isomeric state taken as phenomenological parameters. Therefore, only a rough comparison of the magnetic moments and gyromagnetic factors in both HFBCS and DSM-CQOM approaches can be made.

The results of our reflection-unconstrained calculations are presented in Table III and illustrated in Figs. 3(b) and (c). Summarizing our findings for this part, we note that:

(i) Comparing the total energies obtained for pairing strengths Set 1 ($G_n=16.0$ MeV, $G_p=14.4$ MeV) in Tables II and III we notice that the octupole solutions for the $5/2^{\langle + \rangle}$, $3/2^{\langle + \rangle}$, $5/2^{\langle - \rangle}$ and $7/2^{\langle - \rangle}$ states in Table III appear deeper in energy by 173, 121, 12 and 968 keV, respectively, compared to those in the reflection-symmetric case of Table II. This result favours the presence of octupole deformation in the $5/2^{\langle + \rangle}$, $3/2^{\langle + \rangle}$, and $7/2^{\langle - \rangle}$ states, for which the model predicts non-zero octupole moments. For Set 2 of $G_n=16.5$ MeV, $G_p=14.9$ MeV we observe additional deepening of the total energy

TABLE III: The same as in Table II, and in addition the mass octupole moment Q_{30}^m and deformation β_3^m . All quantities were obtained by reflection-unconstrained (asymmetric) HFBCS calculations for blocked $5/2^{(+)}$, $3/2^{(+)}$, $5/2^{(-)}$ and $7/2^{(-)}$ orbitals in ²²⁹Th with the two different sets of pairing strengths, Set 1 ($G_n = 16.0$ MeV, $G_p = 14.4$ MeV) and Set 2 ($G_n = 16.5$ MeV, $G_p = 14.9$ MeV). The solution for $5/2^{(-)}$ state, obtained with Set 2, corresponds to zero octupole deformation. For each blocked orbital the average parity $\langle \pi \rangle$ is also given. See text for further explanations.

K^{π}	G_p, G_n	$[Nn_z\Lambda](\%)$	$\langle \pi \rangle$	$E_{ m tot}$	E^*	Δ_n	Δ_p	Q_{20}^m	β_2^m	Q_{20}^p	β_2^p	Q_{30}^{m}	β_3^m	μ	g_R	q_s
	Set			(MeV)	(keV)	(MeV)	(MeV)	(fm^2)		(fm^2)		$(b^{3/2})$		(μ_N)		
$\frac{5}{2}\langle + \rangle$	Set 1	[633] (43.3)	0.350	-1743.5399	0.0	0.542	0.814	2107.3	0.213	832.0	0.214	2.369	0.110	0.4254	0.281	0.788
$\overline{2}$	Set 2	[633] (41.7)	0.297	-1743.8174	0.0	0.689	0.933	2107.0	0.213	831.9	0.214	2.141	0.099	0.4181	0.303	0.816
$\frac{3}{2}\langle + \rangle$	Set 1	[631] (22.6)	0.530	-1743.4709	69.0	0.568	0.851	2136.8	0.216	843.7	0.217	1.558	0.072	-0.2729	0.256	0.677
2	Set 2	[631] (23.8)	0.593	-1743.7741	43.3	0.705	0.963	2133.6	0.216	842.5	0.217	1.334	0.062	-0.2635	0.316	0.673
$\frac{5}{2}\langle - \rangle$	Set 1	[752] (23.6)	-0.330	-1743.3379	202.5	0.644	0.885	2144.4	0.217	848.0	0.219	0.182	0.008	0.0408	0.405	0.825
2	Set 2	[752] (35.3)	-1.000	-1743.6968	120.6	0.744	0.986	2140.7	0.216	846.2	0.218	0.000	0.000	-0.2551	0.457	0.716
$\frac{7}{2}\langle - \rangle$	Set 1	[743] (32.5)	-0.370	-1743.4454	94.5	0.581	0.768	2062.0	0.208	815.3	0.210	3.122	0.144	-0.1018	0.400	0.725
$\overline{2}$	Set 2	[743] (32.7)	-0.374	-1743.7197	97.7	0.714	0.881	2049.6	0.207	810.4	0.209	3.004	0.139	-0.0880	0.410	0.719

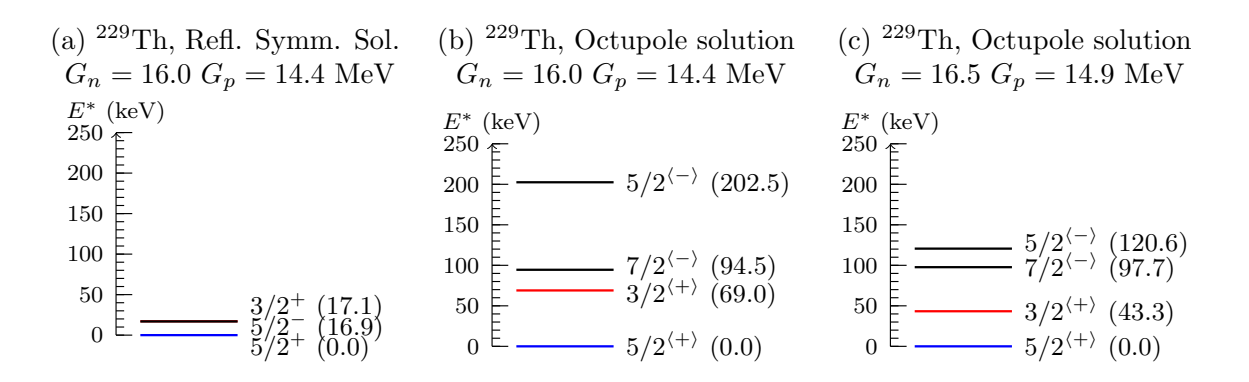


FIG. 3: Lowest one-neutron q.p. excitation energies [see Eq. (1)], in 229 Th calculated in (a) reflection-symmetric (see also Table II) and (b), (c) reflection-unconstrained, asymmetric (see also Table III) Skyrme-SIII HFBCS approximation for two sets of pairing constants. In panel (a) the lines depicting the $3/2^+$ and $5/2^-$ states are degenerate at the given scale and the $7/2^-$ level at 889.4 keV (see Table II) is out of the plot range.

which is essentially due to the change in the pairing energy contribution. The $5/2^{\langle - \rangle}$ state presents the smallest octupole deformation for Set 1 and even zero octupole deformation for Set 2.

(ii) From Table III we notice that the three blocked orbitals appear with mixed average parity. In the $5/2^{\langle + \rangle}$ GS the octupole deformation of $\beta_3 \approx 0.10-0.11$ is obtained a bit larger than that in the $3/2^{\langle + \rangle}$ IS where $\beta_3 \approx 0.06-0.07$. We note that in the DSM-CQOM approach [29] both states are considered with the same quadrupole and octupole deformations $\beta_2 = 0.240$ and $\beta_3 = 0.115$. Comparing the results of the two approaches we notice that the quadrupole deformations obtained for the different states in Table III are a bit smaller than that in DSM-CQOM whereas the octupole deformation in the $5/2^{\langle + \rangle}$ GS appears quite close to that in DSM-CQOM.

(iii) Regarding the excited level spacings, we see in Figs. 3(b) and (c) (see also Table III) that the $3/2^{\langle + \rangle}$ state appears as the lowest excitation corresponding to the isomer with an energy of 69 keV for the Set 1 ($G_n=16.0~{\rm MeV},~G_p=14.4~{\rm MeV}$) and 43 keV for Set 2 ($G_n=16.5~{\rm MeV},~G_p=14.9~{\rm MeV}$). Both values are larger than that in the reflection-symmetric case in Fig. 3(a) (see also Table III), but again, from nuclear structure point of view they correspond to a very-low-energy one-q.p. excitation. However, we note that unlike ²²⁸Th, in ²²⁹Th the fine variation in the pairing constants leads to sizable displacements of the s.p. orbitals resulting in a decrease of about 20 keV in the $3/2^+$ excitation energy. This increased sensitivity of the q.p. spectrum to the pairing strengths (compared to the even-even core nucleus) might be related to the effect of self-consistent

blocking. About the $5/2^{\langle - \rangle}$ excitation we notice that now it appears much higher than the $3/2^{\langle + \rangle}$ state in contrast to the reflection-symmetric case in which the $5/2^-$ state is calculated to be a bit below the $3/2^+$ state [Fig. 3 (a)]. We note that the theoretical values for the $5/2^{\langle - \rangle}$ energy given in Table III for the two (G_n, G_p) sets, 121 keV and 203 keV, now bracket its experimental value of 143 keV [58]. The $7/2^{\langle - \rangle}$ excitation now appears lower, around 90–100 keV, compared to its much higher energy of 889.4 keV obtained in the reflection-symmetric case (Table II). The above results illustrate the importance of both the shape deformation and pairing correlations for the accuracy of the model predictions and the need of their finer treatment for the further quantitative description of 229m Th properties.

(iv) Regarding the GS and IS magnetic moments, we notice that now the obtained GS value $\mu_{\rm GS} \approx 0.42 - 0.43$ μ_N appears lower compared to the reflection-symmetric case, already stepping between the two available (new and old) experimental values of 0.360(7) μ_N [64] and $0.45(4) \mu_N$ [65]. Furthermore, this is the lowest value reached in the DSM-CQOM approach (see Fig. 10(d) in Ref. [31]). At the same time, the calculated isomeric magnetic moment $\mu_{\rm IS}$ of about $-0.27~\mu_N$ underestimates in absolute value the corresponding experimental value of $-0.37(6)\mu_N$ [66, 67]. These results look consistent with the DSM-CQOM calculations [31]. We note, however, that the corresponding spin-gyromagnetic quenching q_s , varying between 0.7 and 0.8 (see Table III), is larger compared to the value of 0.6 considered in [30, 31]. Furthermore, comparing the collective gyromagnetic factor $g_R \approx 0.28 - 0.30$ obtained for $5/2^{\langle + \rangle}$ with the phenomenological ²²⁹Th value of $g_R^{\rm phen} = Z/(Z+N) = 0.393$ we observe a quenching of the latter by a factor of $q_R = g_R/g_R^{\rm phen} \approx 0.71 - 0.76$. For the $3/2^{\langle + \rangle}$ isomer state this quenching factor is $q_R \approx 0.65 - 0.80$. These values are larger than the corresponding ones considered in CQOM-DSM [30, 31]. Thus, it seems that the present calculations are able to approach the corresponding experimental data (especially for the GS) through smaller g_R attenuation (larger q_R). These findings highlight an advantage of the microscopic HFBCS approach over the more phenomenological CQOM-DSM one, since there is no need for phenomenological quenching factors, and the theoretical predictions are close to the experimental values already at smaller attenuation. We note that a more accurate comparison between the two CQOM-DSM and HFBCS approaches can be made on this point after a parity projection is implemented in the latter, although it has been shown that projection after variation affects the total energy only slightly [68].

Concluding on the results obtained so far, the present microscopic approach implemented without particular effort to achieve realistic 229m Th description, shows that the applied HFBCS scheme may carry the basic features needed to study this isomer from a deeper nuclear many-body structure perspective. We emphasize that the quadrupole and octupole deformations β_2 and β_3 are

not free parameters in the EDF approach, but appear as an output of the self-consistent variation procedure. On the other hand, the results obtained suggest that their constraining together with tuning of the pairing strengths at further stage may allow us to determine the proximity of the $5/2^{\langle + \rangle}$ and $3/2^{\langle + \rangle}$ orbitals so as to approach the 229m Th energy scale. At the same time the reasonable values obtained for the magnetic moments show that in a further perspective the model could be able to provide reliable predictions for the B(M1) isomer decay rates. However, the more realistic description of the 229m Th properties within the HFBCS approach requires further development involving Coriolis mixing and appropriate coupling to the collective degrees of freedom as, for example, done in the CQOM-DSM scheme.

IV. CALCULATIONS IN NEIGHBORING NUCLEI

Our results show that the low-energy isomer properties of 229 Th are determined by the position of the $5/2^+$ and $3/2^+$ neutron orbitals near the Fermi level. Thus, it is worth examining the evolution of this condition in the neighboring isotopes, ²²⁷Th and ²³¹Th, as well as in the isotones 227 Ra and 231 U. For each nucleus we calculate the $5/2^+$ and $3/2^+$ neutron q.p. excitation energies together with few neighboring low-lying one-neutron excitations. The basis parameters and pairing constants are determined for the even-even cores (²²⁶Th, ²³⁰Th, ²²⁶Ra and ²³⁰U) by keeping the theoretical moment of inertia [respectively the $E(2_1^+)$ energies] close to the experimental values, following the prescription applied for ²²⁹Th. The numerical results obtained by the reflectionsymmetric and reflection-unconstrained HFBCS calculations are collected in Table IV. Their detailed analysis is given in the following.

A. Neighboring isotopes: ²²⁷Th and ²³¹Th

In 227 Th we found solutions below 1 MeV for the $5/2^+$ and $3/2^+$ orbitals of interest and for the $1/2^+$ orbital. In addition, we find below 1 MeV the $3/2^-$ and $5/2^$ orbitals only in the reflection-symmetric solution, and the $7/2^{\langle - \rangle}$ orbital only in the octupole solution, respectively, as illustrated in Figs. 4(a)-(b). We observe that the reflection-unconstrained solutions appear strongly favored in energy, with the $1/2^{\langle + \rangle}$, $3/2^{\langle + \rangle}$ and $5/2^{\langle + \rangle}$ states lowered by about 1.8 MeV, 0.5 MeV and 0.4 MeV, respectively, with respect to the reflection-symmetric ones (see Table IV). As a result the octupole $1/2^{\langle + \rangle}$ state becomes the ground state, instead of the $5/2^{\langle + \rangle}$ state in ²²⁹Th, in agreement with the experimental data [58]. In all considered states the reflection-asymmetric solution gives large octupole moments and deformations, $\beta_3 \approx 0.13 - 0.15$, suggesting firm octupole deformed shapes in the corresponding excitations. The two states $5/2^+$ and $3/2^+$

TABLE IV: The same as in Tables II and III but for the reflection-symmetric and reflection-unconstrained (octupole) HFBCS solutions for the lowest (below 1 MeV) q.p. states in 227 Th, 227 Ra and 231 U. The symbol "†" marks results of reflection-unconstrained calculations reaching solutions with reflection symmetry.

K^{π}	$E_{ m tot}$	E^*	Δ_n	Δ_p	Q_{20}^m	β_2^m	Q_{20}^p	β_2^p	Q_{30}^{m}	β_3^m	μ	g_R	q_s
	MeV	keV	MeV		$\frac{\text{fm}^2}{\text{Matter}}$		fm^2	* 7 1	$b^{3/2}$		μ_N		
1 +					MeV, G					0, q =		0.004	0.700
$\frac{1}{2}$ 3 +	-1730.0238									_	-0.1017		
$\frac{\bar{2}}{3}$ -	-1730.9523 -1730.8456									_	-0.2968 -0.1110		
$\frac{1}{5}$ +	-1730.8450 -1730.9655				1943.2					_	-0.1110 -0.7080		
$\frac{1}{2} + \frac{1}{2} + \frac{1}{2} + \frac{1}{2} - \frac{1}{2} + \frac{1}{2} - \frac{1}{2}$	-1730.8853 -1730.8853									_	-0.7680 -0.2568	-	
$_{1}^{2}\langle + \rangle$	-1731.7831										-0.0860		
$ \begin{array}{c} \frac{1}{2}\langle + \rangle \\ \frac{1}{2}\langle + \rangle \\ \frac{3}{2}\langle + \rangle \\ \frac{5}{2}\langle + \rangle \\ \frac{7}{2}\langle - \rangle \end{array} $	-1731.4371 -1731.4371												
$\frac{\overline{2}}{5}\langle + \rangle$	-1731.4371 -1731.3871												
$\frac{2}{7}\langle - \rangle$	-1731.4324												
2												0.101	0.100
3+					MeV, G							0.000	0 = 01
$\frac{3}{2} + \frac{5}{2} + \frac{5}{2} - \frac{5}{2}$	-1755.3403				2308.2						-0.3864		
$\frac{3}{2}$ 5 -	-1755.3489				2327.3					_	-0.6816		
$\frac{3}{2}$	-1755.3467				2260.0					_	-0.3160		
$\begin{array}{c} \frac{3}{2}\langle + \rangle \\ \frac{5}{2}\langle + \rangle \dagger \\ \frac{5}{2}\langle - \rangle \dagger \end{array}$	-1755.3746	0.0									-0.3414		
5 (-) †	-1755.3490										-0.6816		
$\frac{3}{2}$	-1755.3467	27.9	0.507	0.894	2260.0	0.225	881.9	0.226	0.000	0.000	-0.3160	0.377	0.721
	2	227 Ra,	$G_n =$	15.9	MeV, G	p = 14	.4 Me	V, b=	= 0.480	0, q =	1.15		
$\frac{5}{2} + \frac{5}{2} + \frac{3}{2} - \frac{5}{2}$	-1731.507	0	0.670	0.893	1914.2	0.197	728.7	0.195	-	-	0.6399	0.202	0.747
$\frac{3}{2}^{+}$	-1731.472	35	0.675	0.894	1910.1	0.196	727.4	0.194	-		-0.3259	0.271	0.760
$\frac{5}{2}$	-1731.458	49	0.668	0.894	1917.3	0.197	730.0	0.195	_	_	-0.2871	0.291	0.710
$\frac{5}{2}\langle + \rangle$	-1731.535	36	0.629	0.804	1921.0	0.197	733.5	0.196	1.699	0.080	0.3504	0.298	0.947
$\frac{3}{2}\langle + \rangle$	-1731.571	0	0.624	0.824	1924.7	0.198	733.6	0.196	1.287	0.061	-0.2484	0.210	0.670
$ \frac{5}{2}\langle + \rangle $ $ \frac{5}{2}\langle + \rangle $ $ \frac{3}{2}\langle + \rangle $ $ \frac{7}{2}\langle - \rangle $	-1731.337	234	0.652	0.774	1884.9	0.193	723.1	0.193	2.585	0.122	-0.1181	0.388	0.734
		²³¹ U.	$G_n =$	15.9 N	MeV, G_1	. = 14	.4 MeV	V. b =	= 0.480	a = 1	1.20		
<u>5</u> -	-1753.612	27			2321.0						-0.2091	0.544	0.717
$\frac{2}{5}$ +	-1753.639	0			2339.5					_	0.8170	0.362	0.731
$\frac{2}{7}$ -	-1752.790	849	0.782	0.840	2359.2	0.234	957.8	0.239	_	_	-0.4024	0.470	0.736
$\frac{5}{2} + \frac{5}{2} + \frac{5}{2} - \frac{7}{2} + \frac{3}{2} + \frac{1}{2}$	-1753.620	19	0.640	0.820	2336.1	0.232	951.1	0.237	_	_	-0.3009	0.420	0.766
$\frac{5}{2}\langle - \rangle \dagger$	-1753.612	70	0.639	0.823	2321.0	0.231	945.3	0.236	0.000	0.000	-0.2091	0.544	0.717
$\begin{array}{c} \frac{5}{2}\langle - \rangle \dagger \\ \frac{5}{2}\langle + \rangle \\ \frac{7}{2}\langle - \rangle \end{array}$	-1753.682	0									0.4623		
$\frac{2}{7}\langle - \rangle$	-1753.559	123									-0.0640		
$\frac{3}{2}\langle + \rangle$	-1753.649	33	0.601	0.825	2326.3	0.231	946.7	0.236	1.065	0.048	-0.2545	0.396	0.676

remain close to one another by only exchanging their positions between the reflection-symmetric and octupole solutions (see Fig. 4).

In 231 Th we find solutions for $3/2^+$, $5/2^+$ and $5/2^-$ neutron q.p. states. In the reflection-unconstrained solutions we observe quite weak signs of octupole deformation. For the $3/2^{(+)}$ state we have an energy gain of only 34 keV with a small octupole deformation of $\beta_3=0.047$.

For $5/2^{\langle + \rangle}$ and $5/2^{\langle - \rangle}$ the reflection-unconstrained solutions appear with zero octupole deformation and coincide with the corresponding reflection-symmetric $5/2^+$ and $5/2^-$ solutions (see Table IV). We note that in the set of reflection-unconstrained results the octupole $3/2^{\langle + \rangle}$ state appears as the GS whereas the experimental data suggests $5/2^+$ as GS [58]. Similarly to 227 Th the two states remain close to one another [see Figs. 4(c)-(d)].

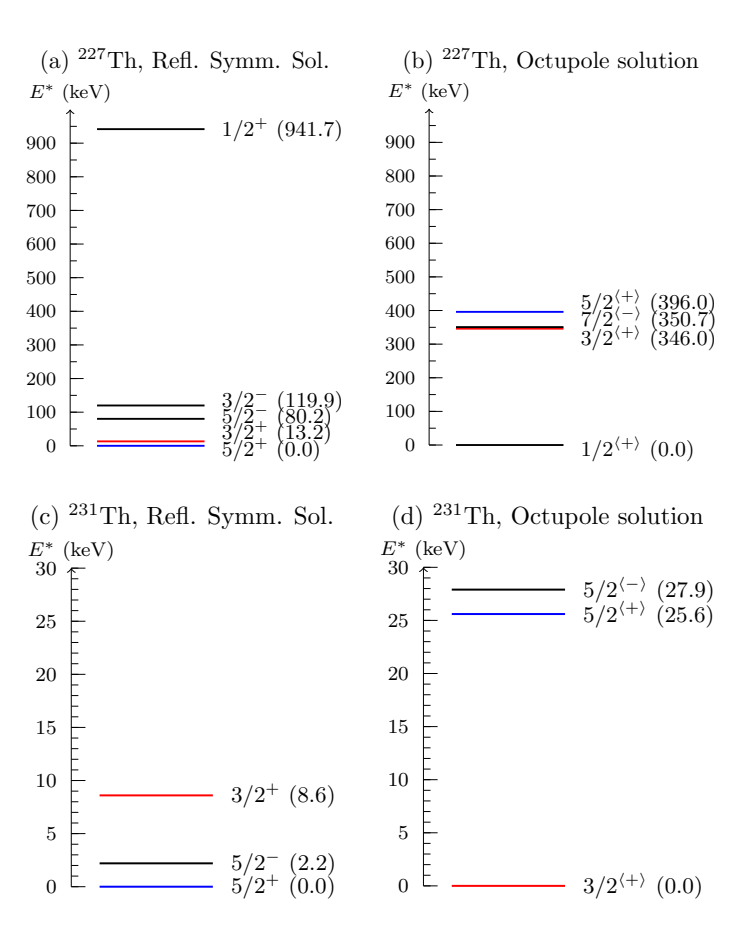


FIG. 4: Lowest one-neutron q.p. excitation energies [given by Eq. (1)] in ²²⁷Th and ²³¹Th calculated in the (a), (c) reflection-symmetric and (b), (d) reflection-unconstrained Skyrme-SIII HFBCS approximation, respectively (see also Table IV). The indistinguishable level bars are identified by the spin labels.

The well pronounced octupole deformation in the ²²⁷Th excitations and the very weak one in ²³¹Th are consistent with the corresponding strong and weak octupole deformations we have observed in the calculations for the even-even core nuclei ²²⁶Th and ²³⁰Th. In turn, this result is consistent with the earlier findings that ²²⁶Th belongs to the region of octupole deformed nuclei around the border of octupole deformation, whereas ²³⁰Th is situated beyond this border, where essentially soft octupole vibrations can be observed [69]. In addition, our calculations in the previous section suggest that ²²⁸Th, the core system of the 229m Th isomer of interest, is the last nucleus towards the N = 82 - 126 midshell in the series of even-even Th isotopes possessing stable octupole deformation in the ground state. This is consistent with the analysis made in Ref. [70] (see Fig. 19 therein). Also, the overall result above suggests that ²²⁹Th may be situated on the border of octupole deformation in the series of odd-mass Thorium isotopes.

B. Neighboring isotones: ²²⁷Ra and ²³¹U

The study of $^{227}\mathrm{Ra}$ and $^{231}\mathrm{U}$, the N=139 isotone neighbours of $^{229}\mathrm{Th}$, is of a special interest due to the same number of neutron orbitals. The core system of the former, $^{226}\mathrm{Ra}$, is also considered to lie around the above mentioned octupole deformation border and one may expect the core of the latter, $^{230}\mathrm{U}$, to have similar reflection-asymmetric characteristics. For $^{227}\mathrm{Ra}$ with experimental GS based on a $K^\pi=3/2^+$ s.p. orbital (the same which determines the $^{229m}\mathrm{Th}$ IS), a very low lying s.p. excitation of 1.7 keV based on the $K^\pi=5/2^+$ orbital (the same which determines the GS of $^{229}\mathrm{Th}$) is reported in [58]. We may therefore expect that the same microscopic mechanism of quasidegeneracy or crossing s.p. orbitals identified in $^{229}\mathrm{Th}$ will play a role for $^{227}\mathrm{Ra}$.

In 231 U the experimental situation given in [58] is highly unclear, with the GS supposed to be $5/2^-$, while a $5/2^+$ state is expected to appear around 40 keV with an uncertainty of 40 keV. No state with $K^{\pi}=3/2^+$ is reported in [58] for this nucleus whereas a 45.1(3) keV state with tentative spin $7/2^-$ is suggested. On the other hand a very recent measurement, related to population

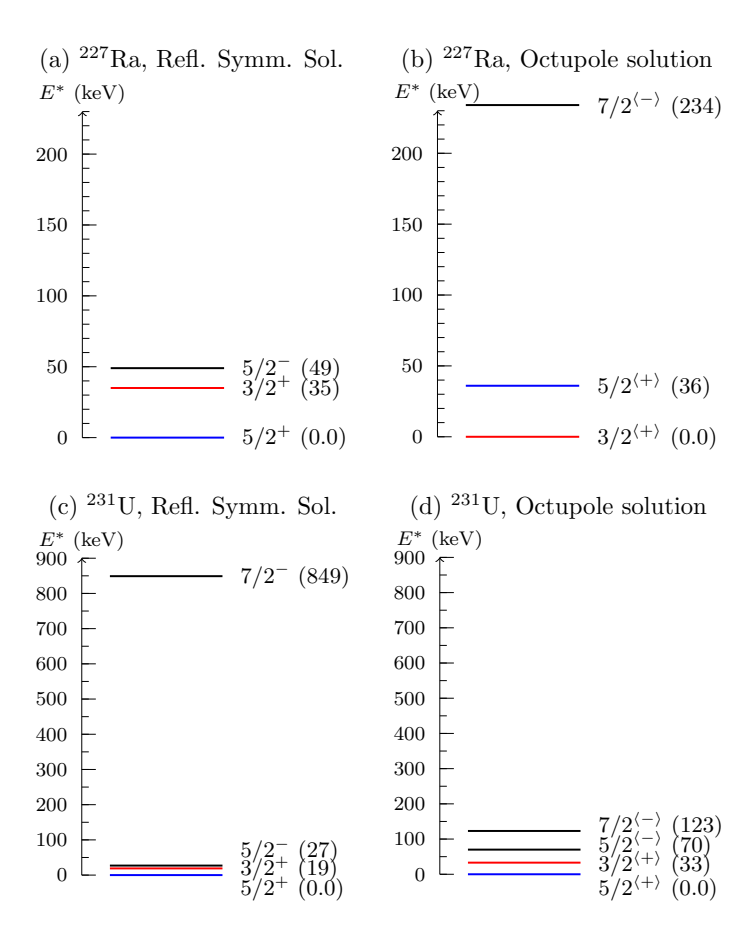


FIG. 5: Same as in Fig. 4, but for ²²⁷Ra and ²³¹U (see also Table IV).

of a rotation band in 231 U [71], suggests that the ground state is based on the neutron $5/2^+$ [633] orbital. Excited bandheads based on the neutron $5/2^-$ [752] and $3/2^+$ [631] orbitals are also suggested there. These spin values and Nilsson quantum numbers coincide with those appearing in the present analysis.

We are therefore confident that the HFBCS calculations in $^{227}\mathrm{Ra}$ and $^{231}\mathrm{U}$ could provide a useful hint on the migration of the $K^{\pi}=5/2^+$ and $3/2^+$ orbitals and their close neighbors aside of $^{229}\mathrm{Th}$ and well as on the evolution of octupole deformation.

In 227 Ra the reflection-symmetric calculations give the $5/2^+$, $3/2^+$ and $5/2^-$ states with the lowest total energies (below 1 MeV) whereas in the reflection-unconstrained calculations $5/2^-$ is replaced by the $7/2^{\langle - \rangle}$ state. This is illustrated in Fig. 5(a)-(b) (see also Table IV). We can make the following observations:

(i) For the $5/2^{\langle + \rangle}$ state the reflection-unconstrained (octupole) solution provides an energy gain of only 28 keV compared to the reflection-symmetric solution, with $\beta_3 = 0.08$. For the $3/2^{\langle + \rangle}$ state the energy gain of the octupole solution is 99 keV with $\beta_3 = 0.06$. For the $7/2^-$ state the calculations suggest some more pronounced octupole deformation with $\beta_3 = 0.12$. Nevertheless, the overall result of the SIII HFBCS calculation suggests for

²²⁷Ra a weaker octupole deformation compared to ²²⁷Th. Also it is weaker than what would be expected, given that in the ²²⁶Ra core calculation we got a rather firm octupole deformation. (Note that the latter is considered as an example of a nucleus with a stable octupole deformation in the ground state even though situated around the border of octupole collectivity [72, 73].) This might be a hint for a stronger influence of the odd neutron under the condition of a different proton number (compared to ²²⁷Th) on the even-even core leading to a softer octupole deformation. More detailed studies (beyond the scope of this work) of the s.p. structure provided by the mean field in this region may be necessary to understand this result.

(ii) Despite the above discussion concerning the octupole deformation, the calculations show that in the reflection-symmetric case the $5/2^+$ state appears to be the GS, whereas in the octupole case the GS is given by the $3/2^{\langle + \rangle}$ state (see Fig. 5). The latter is favored, even though just slightly, by the values of the total energy and in addition by the assignment in Ref. [58] which suggests the 227 Ra GS with $K^{\pi}=3/2^+$. Also, the octupole calculation favors $5/2^{\langle + \rangle}$ as the first excited q.p. state, again in corroboration with the experiment [58]. We note that its excitation energy is obtained to be small (36 keV),

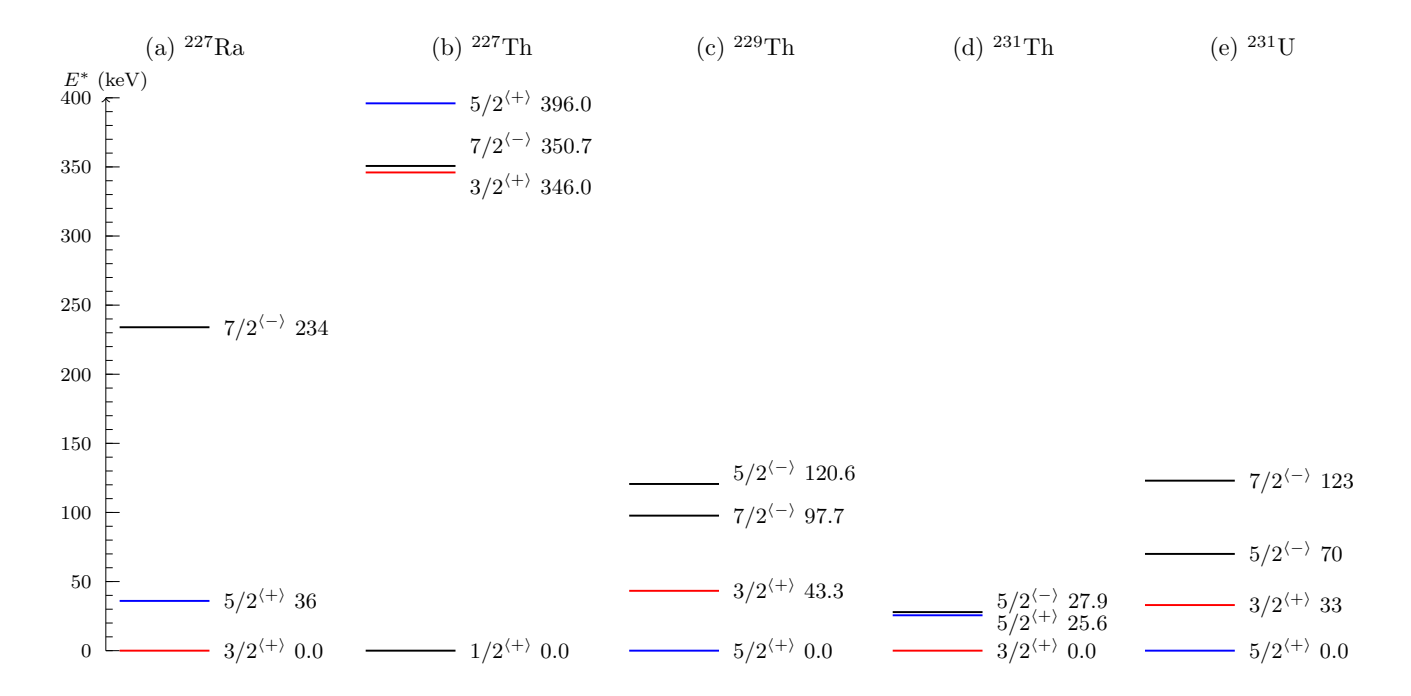


FIG. 6: Lowest one-neutron q.p. excitation energies [given in Eq. (1)] in 227 Th, 229 Th, 231 Th, 227 Ra and 231 U calculated in the reflection-unconstrained Skyrme-SIII HFBCS approximation are given to follow the evolution of the $K^{\pi}=5/2^{+}$ and $K^{\pi}=3/2^{+}$ states around 229 Th (see also Table IV).

relatively close to experiment (1.7 keV).

- (iii) We note that the magnetic moment obtained for the $3/2^{\langle + \rangle}$ ground state in the reflection-unconstrained calculation takes the value of $-0.248~\mu_N$ which considerably underestimates in absolute value the experimental value of $-0.404(2)~\mu_N$ [74]. On the other hand the value of $-0.326~\mu_N$ obtained in the symmetric solution for the $3/2^+$ state is closer to the experiment.
- (iv) The above overall results show that by moving from 229 Th to 227 Ra under the condition of reflection asymmetry, the $5/2^+$ and $3/2^+$ orbitals exchange their roles in the ground and first excited q.p. state but still remain close to one another. The mutual rearrangement of these two orbitals is similar to what was observed in 227 Th and 231 Th.

We now turn to the case of 231 U, where both the reflection-symmetric and reflection-unconstrained calculations give the low-lying q.p. excitations with $5/2^-$, $5/2^+$, $7/2^-$ and $3/2^+$, as seen in Table IV and Fig. 5(c)-(d). Here we can make the following comments:

(i) We see that in both reflection-symmetric and octupole calculations, the ground state is obtained with $K^{\pi}=5/2^+$ and not with the $K^{\pi}=5/2^-$ quantum number adopted in the experimental database [58]. However, as noted above, the very recent measurement [71] suggests that the ground state is based on the neutron $5/2^+[633]$ orbital thus corroborating our result. Our first excited state is $K^{\pi}=3/2^+$, then comes $K^{\pi}=5/2^-$ and finally $K^{\pi}=7/2^-$. We note that in both cases the obtained $K^{\pi}=5/2^+$ GS and the first excited $K^{\pi}=3/2^+$

state remain rather close to one another (see Fig. 5).

- (ii) Except for $K^{\pi}=5/2^{\langle -\rangle}$ the calculations provide lower total energy in the case of reflection-unconstrained solutions (see Table IV). Thus, the octupole ground state $K^{\pi}=5/2^{\langle +\rangle}$ and the $K^{\pi}=3/2^{\langle +\rangle}$ excitation appear slightly favored by 43 keV and 29 keV, respectively, with respect to the reflection symmetric case. At the same time, the $K^{\pi}=7/2^{\langle -\rangle}$ state goes deeper by 769 keV with a large $\beta_3=0.151$. For $K^{\pi}=5/2^{\langle -\rangle}$ the reflection-unconstrained calculation does not differ from the symmetric solution with $\beta_3=0$.
- (iii) We notice that in most of the considered states, both calculations (reflection-symmetric and octupole) give quite large values for the collective gyromagnetic factor g_R exceeding the phenomenological Z/A=0.398 ratio for $^{231}\mathrm{U}$, while usually they would be expected to be smaller. Further detailed work is needed to understand this result.

Finally, we would like to note that we refrain from comparing in our analysis the theoretical excited state energies with experimental values for bandheads with the same angular momentum, which are for some cases available and might show considerable energy differences. The main reason is that in all cases the excited bandheads, especially those at relatively high energy of few hundreds of keV, are coupled to other dynamical modes—collective vibrations and rotations with possible Coriolis mixing effects, as well—which are not included in the present theoretical modeling. Presently the only possible way to better describe available excited states could be through

variation of the pairing parameters trying to adjust them to reproduce the lowest one-q.p. excitation, in particular the 229m Th isomer, instead of relying on the adjustment to the core moment of inertia. However, such an attempt is beyond the scope of this work.

Summarizing the result of calculations in the ^{227,231}Th isotopes and ²²⁷Ra, ²³¹U isotones, we remark that the pair of $K^{\pi} = 5/2^+$ and $K^{\pi} = 3/2^+$ orbitals sustainedly plays a role in the formation of low-lying excitations in the nuclei around ²²⁹Th. This is illustrated in Fig. 6 where we collect and compare the low-lying one-neutron q.p. levels obtained for all considered nuclei in the case of reflection-unconstrained HFBCS calculations. We also note that in our calculations the two orbitals mentioned above, together with the few other neighboring orbitals considered, keep the same Nilsson quantum numbers in the leading components of the corresponding s.p. wave functions as in ²²⁹Th (see Tables II and III). The observed evolution of the intrinsic structure in the vicinity of ²²⁹Th suggests that the same microscopic mechanism for formation of low-energy excitations, involving s.p. orbital-crossing or quasi-degeneracy, may govern in combination with other degrees of freedom, such as collective vibrations and rotations, the appearance of similar low-energy isomeric states in the same mass region. Furthermore, a search for the appearance of similar intrinsicstructure conditions in other mass regions seems to be worth doing.

V. CONCLUSION AND PERSPECTIVES

We applied a Skyrme HFBCS approach to study the microscopic grounds of the ^{229m}Th isomer-formation mechanism and its possible manifestation in other nuclei. By properly handling the pairing, moment-of-inertia and quadrupole-octupole shape characteristics inherent to actinide nuclei we expanded stepwise the study over the even-even core and core-plus-particle intrinsic structures of ²²⁹Th and its closest odd-isotope ²²⁷Th, ²³¹Th and odd-isotone ²²⁷Ra, ²³¹U neighbors. Focusing on the isomer-forming s.p. orbitals and their neighboring orbitals, we examined the related low-lying q.p. excitations and the deformation and intrinsic moment characteristics in ²²⁹Th and around. We reach the following conclusions:

- (i) The model calculation with the Skyrme SIII parametrization provides the necessary orbitals in the s.p. spectrum of the even-even core nucleus $^{228}{\rm Th}$ and subsequently the correct order of the ground $K^\pi=5/2^+$ and first excited $K^\pi=3/2^+$ states in $^{229}{\rm Th}$ promoting the latter as the model candidate for the isomer in both cases of reflection symmetry and octupole deformation.
- (ii) The reflection-unconstrained (octupole) solutions provide lower total energy in all considered states of 229 Th compared to the reflection-symmetric solutions. On the other hand, the latter provide lower $3/2^+$ excitation energy for 229 Th, however for all considered cases orders of magnitude larger than the 8 eV experimental

isomer energy. Allegedly, eV accuracy is out of reach of current nuclear models. Within the typically nuclear energy scale accuracy, we adopt the $3/2^+$ energy of about 40 keV from the octupole solution in Table III as the current SIII-HFBCS prediction for the 229m Th isomer.

- (iii) The reflection-symmetric solution significantly overestimates the experimental 229 Th GS magnetic moment while reproducing the IS magnetic moment within the experimental uncertainties. On the other hand, the octupole solution approaches the GS magnetic moment from above while slightly overestimating the IS magnetic moment. Overall, this result is very similar to the corresponding magnetic moment descriptions obtained in the CQOM-DSM approach [29, 31] and in earlier DSM calculations [75]. This consistency suggests that the Skyrme-SIII HFBCS calculation may provide the relevant s.p. wave functions capable of predicting reasonably well the B(M1) radiative decay rate of 229m Th.
- (iv) The analysis of the spacings between the lowest excited bandheads obtained in 229 Th shows a stability of the model predictions for the quadrupole and octupole moments, deformation parameters and magnetic moments as well, compared to energy-level shifts of tens of keVs caused by the variation in the pairing strengths. It follows that within such limits of $3/2^+$ energy-level variation the obtained HFBCS predictions for the considered observables may provide reasonable qualitative characterization of the 229m Th isomer-formation conditions. Moreover, this suggests that further model calculations involving the B(M1) transition rates could also carry valuable microscopic information about the $3/2^+$ isomer-decay regardless of the keV-limited accuracy.
- (v) The application of the SIII-HFBCS approach to the odd isotope and isotone neighbors of ²²⁹Th suggests a plausible evolution of the considered excitations in the actinide region of the nuclear chart. In $^{227}\mathrm{Ra}$ and $^{231}\mathrm{Th}$ the calculations suggest $3/2^+$ as the ground state, while setting $5/2^+$ as the first excited state, thus exchanging their roles as compared to 229 Th. At the same time 231 U presents the same level order as 229 Th, with $5/2^+$ being the GS and $3/2^+$ appearing as the first excitation. In $^{227}\mathrm{Th}$ the calculations indicate a strong octupole deformation which essentially rearranges the levels pushing both $5/2^{\langle + \rangle}$ and $3/2^{\langle + \rangle}$ upper in energy and setting $1/2^{\langle + \rangle}$ as the GS in agreement with experiment. An interesting byproduct of our calculations is that ²²⁹Th appears at the border of octupole deformation in the series of odd-mass Thorium isotopes. The observed "migration" of other neighboring states, such as $5/2^-$ and $7/2^-$, around suggests a potential rearrangement of the s.p. orbitals, including crossing and quasi-degeneracy, in a way providing conditions for the appearance of yet not experimentally observed extremely low-energy excitations.

The main conclusion of the study is that the present Skyrme EDF approach gives us a basis for a deeper microscopic understanding of the mechanism which governs the formation of low and eventually extremely low-lying nuclear excitations. Our results point on the good spectroscopic quality of the SIII interaction in ²²⁹Th and its odd-mass neighbors. In this aspect it would be also interesting to test other Skyrme parametrizations, especially such with effective mass close to one, known to be successful in reproducing single-particle spectra around the Fermi level. At the same time the further practical application of the approach on a quantitative level (apart from the possible tuning of pairing constants) requires a few developments in different directions. First, the inclusion of the Coriolis coupling between the odd nucleon and the core (implying a sophisticated evaluation of the core moment of inertia and relevant intrinsic matrix element) with the K-mixing effect allowing for the M1 decay and additional coupling to collective rotation and/or vibration modes allowing for electric E2 and E1 or E3 transitions. Further, detailed implementation of nuclear shape effects, parity projection, moments of inertia and gyromagnetic characteristics within a unified particle-core framework will be necessary to reach a quantitative description and prediction of energy and electromagnetic properties of ^{229m}Th on a level of accuracy comparable with the more phenomenological schemes such as the CQOM-DSM. This development could be the subject of further work.

ACKNOWLEDGMENTS

The authors would like to thank P. G. Reinhard for fruitful discussions. This work is supported by the Bulgarian National Science Fund (BNSF) under Contract No. KP-06-N48/1. N.M. acknowledges with thanks the use of the MPIK-Heidelberg computer cluster allowed through a collaboration with the Division of Prof. Dr. Klaus Blaum. AP gratefully acknowledges support from the Deutsche Forschungsgemeinschaft (DFG, German Science Foundation) in the framework of the Heisenberg Program (PA 2508/3-1) and from the ThoriumNuclearClock project that has received funding from the European Research Council (ERC) under the European Union's Horizon 2020 research and innovation programme (Grant Agreement No. 856415).

Appendix A: Minimal scheme of time-odd terms in Skyrme energy-density functional

First, we recall here the expressions of the central, density-dependent and spin-orbit parts of the energy-density functional, omitting the coordinate \mathbf{r} dependence

of local densities to shorten the expressions

$$\mathcal{H}_{c}(\mathbf{r}) = B_{1} \rho^{2} + B_{10} \mathbf{s}^{2} + B_{3} (\rho \tau - \mathbf{j}^{2})$$

$$+ B_{14} (\overrightarrow{\mathbf{J}}^{2} - \mathbf{s} \cdot \mathbf{T}) + B_{5} \rho \Delta \rho + B_{18} \mathbf{s} \cdot \Delta \mathbf{s}$$

$$+ \sum_{q=n,p} \left\{ B_{2} \rho_{q}^{2} + B_{11} \mathbf{s}_{q}^{2} + B_{4} (\rho_{q} \tau_{q} - \mathbf{j}_{q}^{2}) + B_{15} (\overrightarrow{\mathbf{J}}_{q}^{2} - \mathbf{s}_{q} \cdot \mathbf{T}_{q}) + B_{6} \rho_{q} \Delta \rho_{q} + B_{19} \mathbf{s}_{q} \cdot \Delta \mathbf{s}_{q} \right\}, \qquad (A1a)$$

$$\mathcal{H}_{DD}(\mathbf{r}) = \rho^{\alpha} \left[B_{7} \rho^{2} + B_{12} \mathbf{s}^{2} + \sum_{q=n,p} \left(B_{8} \rho_{q}^{2} + B_{13} \mathbf{s}_{q}^{2} \right) \right], \qquad (A1b)$$

$$\mathcal{H}_{s.o.}(\mathbf{r}) = B_{9} \left[\rho \nabla \cdot \mathbf{J} + \mathbf{j} \cdot \nabla \times \mathbf{s} + \sum_{q=n,p} \left(\rho_{q} \nabla \cdot \mathbf{J}_{q} + \mathbf{j}_{q} \cdot \nabla \times \mathbf{s}_{q} \right) \right], \qquad (A1c)$$

where the index q in local densities is the charge state (q = n for neutrons or q = p for protons). In Eq. (A1a), $\overrightarrow{J_q}^2 = J_{q,\mu\nu} J_q^{\mu\nu}$ (using Einstein's summation convention) and in Eq. (A1c) \mathbf{J}_q denotes the antisymmetric part of the spin-current tensor $J_q^{\mu\nu}$ [76]. The coupling constants B_i are related to the Skyrme parameters by expressions given, e.g., in Ref. [77]. The time-even local densities $\rho(\mathbf{r})$, $\tau(\mathbf{r})$ and $J_{\mu\nu}(\mathbf{r})$ appearing in Eqs. (A1a) to (A1c) are defined in terms of the spinor wave functions $[\psi_k](\mathbf{r})$ of the Hartree–Fock basis states by

$$\rho(\mathbf{r}) = \sum_{k} v_k^2 \left[\psi_k \right]^{\dagger} (\mathbf{r}) [\psi_k] (\mathbf{r}) , \qquad (A2a)$$

$$\tau(\mathbf{r}) = \sum_{k} v_k^2 \left(\nabla [\psi_k]^{\dagger}(\mathbf{r}) \right) \cdot \nabla [\psi_k](\mathbf{r}) , \qquad (A2b)$$

$$J_{\mu\nu}(\mathbf{r}) = \frac{1}{2i} \sum_{k} v_k^2 \left\{ [\psi_k]^{\dagger}(\mathbf{r}) \, \sigma_{\nu} \partial_{\mu} [\psi_k](\mathbf{r}) \right.$$

$$-\left(\partial_{\mu}[\psi_{k}]^{\dagger}(\mathbf{r})\right)\sigma_{\nu}[\psi_{k}](\mathbf{r})\right\}, \quad (A2c)$$

whereas the relevant time-odd densities $\mathbf{s}(\mathbf{r})$, $T_{\mu}(\mathbf{r})$ and $\mathbf{j}(\mathbf{r})$ respectively read

$$\mathbf{s}(\mathbf{r}) = \sum_{k} v_k^2 \left[\psi_k \right]^{\dagger}(\mathbf{r}) \, \sigma[\psi_k](\mathbf{r}) \,, \tag{A3a}$$

$$T_{\mu}(\mathbf{r}) = \sum_{k} v_{k}^{2} \left(\nabla [\psi_{k}]^{\dagger}(\mathbf{r}) \right) \cdot \sigma_{\mu} \nabla [\psi_{k}](\mathbf{r}) , \qquad (A3b)$$

$$\mathbf{j}(\mathbf{r}) = \frac{1}{2i} \sum_{k} v_k^2 \left\{ \left(\nabla [\psi_k]^{\dagger}(\mathbf{r}) \right) [\psi_k](\mathbf{r}) \right.$$

$$- [\psi_k]^{\dagger}(\mathbf{r}) \nabla [\psi_k](\mathbf{r}) \right\}. \tag{A3c}$$

It is worth noting that the summation runs over all the Hartree–Fock basis without assuming any specific relation between the wave functions of canonically conjugate states because of time-reversal symmetry breaking at the one-body level.

The Hartree–Fock one-body Hamiltonian $\hat{h}_{\mathrm{HF}}^{(q)}$ takes the following form in coordinate representation for the charge state q

$$\langle \mathbf{r} | \hat{h}_{\mathrm{HF}}^{(q)} | \psi_{k} \rangle = - \nabla \cdot \left[\left(\frac{\hbar^{2}}{2m_{q}^{*}(\mathbf{r})} + \mathbf{C}_{q}(\mathbf{r}) \cdot \sigma \right) \nabla [\psi_{k}](\mathbf{r}) \right]$$

$$+ \left(U_{q}(\mathbf{r}) + \delta_{q p} V_{\mathrm{Coul}}(\mathbf{r}) \right) [\psi_{k}](\mathbf{r})$$

$$+ i \mathbf{W}_{q}(\mathbf{r}) \cdot \left(\sigma \times \nabla [\psi_{k}](\mathbf{r}) \right)$$

$$- i \left[W_{q}^{\mu\nu}(\mathbf{r}) \sigma_{\nu} \partial_{\mu} [\psi_{k}](\mathbf{r}) \right]$$

$$+ \nabla_{\mu} \left(W_{q}^{\mu\nu}(\mathbf{r}) \sigma_{\nu} [\psi_{k}](\mathbf{r}) \right)$$

$$- i \mathbf{A}_{q}(\mathbf{r}) \cdot \nabla [\psi_{k}](\mathbf{r}) + \mathbf{S}_{q}(\mathbf{r}) \cdot \sigma [\psi_{k}](\mathbf{r}) .$$

$$(A4)$$

The time-even fields $m_q^*(\mathbf{r})$, $U_q(\mathbf{r})$, $V_{\text{Coul}}(\mathbf{r})$, $\mathbf{W}_q(\mathbf{r})$ and $W_q^{\mu\nu}(\mathbf{r})$ denote the effective-mass field, the central-plus-density-dependent field, the Coulomb field, the spin-orbit field and the spin-current field respectively, whereas $\mathbf{S}_q(\mathbf{r})$, $\mathbf{A}_q(\mathbf{r})$ and $\mathbf{C}_q(\mathbf{r})$ are time-odd fields. The expressions of all the fields can be found in, e.g., Refs. [39, 77], but we recall here those relevant for the "minimal scheme" definition

$$W_{q}^{\mu\nu}(\mathbf{r}) = B_{14}J^{\mu\nu} + B_{15}J_{q}^{\mu\nu} , \qquad (A5a)$$

$$\mathbf{S}_{q}(\mathbf{r}) = 2(B_{10} + B_{12}\rho^{\alpha})\mathbf{s} + 2(B_{11} + B_{13}\rho^{\alpha})\mathbf{s}_{q}$$

$$- B_{9}\nabla \times (\mathbf{j} + \mathbf{j}_{q}) - B_{14}\mathbf{T} - B_{15}\mathbf{T}_{q}$$

$$+ 2(B_{18}\Delta\mathbf{s} + B_{19}\Delta\mathbf{s}_{q}) , \qquad (A5b)$$

$$\mathbf{A}_{q}(\mathbf{r}) = -2(B_{3}\mathbf{j} + B_{4}\mathbf{j}_{q}) + B_{9}\nabla \times (\mathbf{s} + \mathbf{s}_{q}) , \qquad (A5c)$$

$$\mathbf{C}_{q}(\mathbf{r}) = -B_{14}\mathbf{s} - B_{15}\mathbf{s}_{q} . \qquad (A5d)$$

In this context, the so-called "minimal scheme" for the Skyrme SIII parametrization is then defined by the neglect, in the energy density functional as well as in the Hartree–Fock potential, of

- the B_{14} and B_{15} terms because they were not included in the fit of Skyrme SIII parameters;
- the B_{18} and B_{19} terms because they may yield finite-size spin instabilities according to Ref. [77].

Therefore, the local densities $W_q^{\mu\nu}(\mathbf{r})$ and $\mathbf{T}_q(\mathbf{r})$, as well as the Laplacian of the spin density, $\Delta \mathbf{s}_q(\mathbf{r})$, are not involved in our calculations with SIII. As a consequence, the field $\mathbf{C}_q(\mathbf{r})$, which adds a spin-dependent contribution to the effective-mass field, and the field $W_q^{\mu\nu}(\mathbf{r})$, introducing a tensor contribution to the spin-orbit potential, disappear from the Hartree–Fock Hamiltonian in Eq. (A4). The only time-odd contributions to $\hat{h}_{\mathrm{HF}}^{(q)}$ thus come from the current field $\mathbf{A}_q(\mathbf{r})$ and the spin field $\mathbf{S}_q(\mathbf{r})$ reduced to

$$\mathbf{S}_{q}(\mathbf{r}) \approx 2(B_{10} + B_{12} \rho^{\alpha}) \mathbf{s} + 2(B_{11} + B_{13} \rho^{\alpha}) \mathbf{s}_{q} - B_{9} \nabla \times (\mathbf{j} + \mathbf{j}_{q}).$$
(A6)

Appendix B: Quadrupole and octupole moments and deformation parameters in the HFBCS calculation

In the HFBCS algorithm of Ref. [39] the quadrupole deformation parameter β can be determined in two ways, through the mass (m) or charge (p - proton) quadrupole moments and radii, as follows:

$$\beta_2^m = \sqrt{\frac{\pi}{5}} \frac{\langle \hat{Q}_{20}^m \rangle}{3 \langle r_m^2 \rangle} , \qquad (B1)$$

$$\beta_2^p = \sqrt{\frac{\pi}{5}} \frac{\langle \hat{Q}_{20}^p \rangle}{Z \langle r_p^2 \rangle} , \qquad (B2)$$

where \widehat{Q}_{20}^m (\widehat{Q}_{20}^p) and $\langle r_m^2 \rangle$ ($\langle r_p^2 \rangle$) are the mass (charge) quadrupole momenta and mean quadratic radii calculated in the code as

$$\langle \widehat{Q}_{20}^m \rangle = \int d\mathbf{r} \, \rho(\mathbf{r}) \left(3z^2 - \mathbf{r}^2 \right) ,$$
 (B3)

$$\langle \widehat{Q}_{20}^p \rangle = \int d\mathbf{r} \, \rho_p(\mathbf{r}) \left(3z^2 - \mathbf{r}^2 \right) \,,$$
 (B4)

and

$$\langle r_m^2 \rangle = \frac{1}{A} \int d\mathbf{r} \, \rho(\mathbf{r}) \, \mathbf{r}^2 \,,$$
 (B5)

$$\langle r_p^2 \rangle = \frac{1}{Z} \int d\mathbf{r} \, \rho_p(\mathbf{r}) \, \mathbf{r}^2 \,,$$
 (B6)

where $\rho(\mathbf{r})$ and $\rho_p(\mathbf{r})$ are the total (mass) and proton (charge) densities, respectively, and $\mathbf{r}^2 = z^2 + x^2 + y^2$. The mass and charge densities $\rho(\mathbf{r})$ and $\rho_p(\mathbf{r})$ are basic ingredients of the HFBCS solution (see Eq. (A2a) for the definition of the former, whereas the restriction in the summation to proton states gives $\rho_p(\mathbf{r})$). In the calculation in formula (B2) the charge mean quadratic radii $\langle r_p^2 \rangle$ are corrected by the addition of the value $a^2 = (0.85)^2$ fm² taking into account the proton radius.

The octupole deformation is calculated from the mass and charge octupole moments as

$$\beta_3^m = \frac{4\pi}{3AR_0^3} \langle \widehat{\overline{Q}}_{30}^m \rangle , \qquad (B7)$$

$$\beta_3^p = \frac{4\pi}{3ZR_0^3} \langle \widehat{\overline{Q}}_{30}^p \rangle , \qquad (B8)$$

where

$$\langle \widehat{\overline{Q}}_{30}^m \rangle = \frac{1}{2} \sqrt{\frac{7}{4\pi}} \int d\mathbf{r} \, \rho(\mathbf{r}) \, z(2z^2 - 3x^2 - 3y^2), \, (B9)$$

$$\langle \widehat{\overline{Q}}_{30}^p \rangle = \frac{1}{2} \sqrt{\frac{7}{4\pi}} \int d\mathbf{r} \, \rho_p(\mathbf{r}) \, z (2z^2 - 3x^2 - 3y^2) (B10)$$

Here, $R_0 = r_0 A^{1/3}$ with $r_0 = 1.2$ fm.

The above expressions (B1), (B2) and (B7), (B8) illustrate the particular way in which the quadrupole and octupole moments and deformation parameters are calculated in the present HFBCS algorithm. They can be

also written in a more unified form and also related to different forms used in other works.

Thus, we remark that Eqs. (B1) and (B2) can be approximately written in terms of R_0 as in the case of Eqs. (B7) and (B8). Considering that for small quadrupole deformations one can approximate the mean square radius $\langle r^2 \rangle$, similarly to the radius of a system of A particles in a spherical harmonic oscillator potential, as (see Eq. (2.11) on p. 41 of Ref. [78])

$$\langle r^2 \rangle = \frac{1}{A} \sum_{i=1}^{A} \langle r^2 \rangle_i \simeq \frac{3}{5} \left(r_0 A^{1/3} \right)^2 = \frac{3}{5} R_0^2 , \quad \text{(B11)}$$

and substituting it into Eqs. (B1) and (B2) one gets

$$\beta_2^m = \frac{\sqrt{5\pi}}{3AR_0^2} \langle \widehat{Q}_{20}^m \rangle = \frac{\sqrt{5\pi}}{3r_0^2 A^{5/3}} \langle \widehat{Q}_{20}^m \rangle , \quad (B12)$$

$$\beta_2^p = \frac{\sqrt{5\pi}}{3ZR_0^2} \langle \widehat{Q}_{20}^p \rangle = \frac{\sqrt{5\pi}}{3Zr_0^2 A^{2/3}} \langle \widehat{Q}_{20}^p \rangle .$$
 (B13)

Eq. (B12) corresponds to Eq. (34) in [79] and Eq. (3) of [80], while Eq. (B13) corresponds to Eq. (1.72) in Ref. [78] and, e.g., Eq. (11) in Ref. [81] up to the first order of β_2 .

Regarding the octupole moments and deformation parameters, if we consider

$$\langle \widehat{\overline{Q}}_{30} \rangle = \frac{1}{2} \sqrt{\frac{7}{4\pi}} \langle \widehat{Q}_{30} \rangle, \tag{B14}$$

with

$$\langle \widehat{Q}_{30} \rangle = \int d\mathbf{r} \, \rho(\mathbf{r}) \, z(2z^2 - 3x^2 - 3y^2),$$
 (B15)

one obtains

$$\beta_3^m = \frac{\sqrt{7\pi}}{3AR_0^3} \langle \widehat{Q}_{30}^m \rangle , \qquad (B16)$$

$$\beta_3^p = \frac{\sqrt{7\pi}}{3ZR_0^3} \langle \widehat{Q}_{30}^p \rangle . \tag{B17}$$

Thus, Eq. B7 corresponds to Eq. (34) in [79] and Eq. (4) of [80], while Eq. (B8) corresponds to Eq. (6) in Ref. [72].

Also, we remark that the expectation values of the quadrupole and octupole operators in Eqs. (B3), (B4) and (B15), respectively, correspond to Eqs. (1) and (2) in [80], respectively, as well as to those in Eq. (35) of Ref. [79].

Finally, unifying Eq. (B12) with Eq. (B16) and Eq. (B13) with Eq. (B17) we obtain

$$\beta_{\lambda}^{m} = \frac{\sqrt{(2\lambda + 1)\pi}}{3AR_{0}^{\lambda}} \langle \widehat{Q}_{\lambda 0}^{m} \rangle , \qquad (B18)$$

$$\beta_{\lambda}^{p} = \frac{\sqrt{(2\lambda + 1)\pi}}{3ZR_{0}^{\lambda}} \langle \widehat{Q}_{\lambda 0}^{p} \rangle , \qquad (B19)$$

with $\lambda=2,3,$ where Eq. (B19) corresponds to Eq. (2.23) in Ref. [82].

- [1] E. Peik and Chr. Tamm, Europhys. Lett. 61, 181 (2003),
 URL https://doi.org/10.1209/epl/i2003-00210-x.
- [2] C. J. Campbell, A. G. Radnaev, A. Kuzmich, V. A. Dzuba, V. V. Flambaum, and A. Derevianko, Phys. Rev. Lett. 108, 120802 (2012), URL https://link.aps.org/doi/10.1103/PhysRevLett.108.120802.
- [3] E. Peik and M. Okhapkin, Comptes Rendus Physique 16, 516 (2015), URL http://www.sciencedirect.com/ science/article/pii/S1631070515000213.
- [4] V. V. Flambaum, Phys. Rev. Lett. 97, 092502 (2006), URL https://link.aps.org/doi/10.1103/PhysRevLett.97.092502.
- [5] P. Fadeev, J. C. Berengut, and V. V. Flambaum, Phys. Rev. A 102, 052833 (2020), URL https://link.aps. org/doi/10.1103/PhysRevA.102.052833.
- [6] E. Peik, T. Schumm, M. Safronova, A. Pálffy, J. Weitenberg, and P. G. Thirolf, Quantum Science and Technology 6, 034002 (2021).
- [7] Y.-D. Tsai, J. Eby, and M. S. Safronova, Nature Astronomy 7, 113 (2023).
- [8] B. R. Beck, J. A. Becker, P. Beiersdorfer, G. V. Brown, K. J. Moody, J. B. Wilhelmy, F. S. Porter, C. A. Kilbourne, and R. L. Kelley, Phys. Rev. Lett.

- 98, 142501 (2007), URL https://link.aps.org/doi/10.1103/PhysRevLett.98.142501.
- [9] B. R. Beck, C. Y. Wu, P. Beiersdorfer, G. V. Brown, J. A. Becker, K. J. Moody, J. B. Wilhelmy, F. S. Porter, C. A. Kilbourne, and R. L. Kelley, in 12th International Conference on Nuclear Reaction Mechanisms (Varenna, Italy, 2009), vol. LLNL-PROC-415170.
- [10] B. Seiferle et al., Nature (London) **573**, 243 (2019).
- [11] A. Yamaguchi et al., Phys. Rev. Lett. 123, 222501 (2019).
- [12] T. Sikorsky, J. Geist, D. Hengstler, S. Kempf, L. Gastaldo, C. Enss, C. Mokry, J. Runke, C. E. Düllmann, P. Wobrauschek, et al., Phys. Rev. Lett. 125, 142503 (2020), URL https://journals.aps.org/prl/ abstract/10.1103/PhysRevLett.125.142503.
- [13] S. Kraemer, J. Moens, M. Athanasakis-Kaklamanakis, S. Bara, K. Beeks, P. Chhetri, K. Chrysalidis, A. Claessens, T. E. Cocolios, J. G. Correia, et al., Nature 617, 706 (2023).
- [14] J. Tiedau, M. V. Okhapkin, K. Zhang, J. Thielking, G. Zitzer, E. Peik, F. Schaden, T. Pronebner, I. Morawetz, L. T. De Col, et al., Phys. Rev. Lett. 132, 182501 (2024), URL https://link.aps.org/doi/

- 10.1103/PhysRevLett.132.182501.
- [15] L. von der Wense, B. Seiferle, M. Laatiaoui, J. B. Neumayr, H.-J. Maier, H.-F. Wirth, C. Mokry, J. Runke, K. Eberhardt, C. E. Düllmann, et al., Nature 533, 47 (2016), ISSN 0028-0836, article, URL http://dx.doi.org/10.1038/nature17669.
- [16] B. Seiferle, L. von der Wense, and P. G. Thirolf, Phys. Rev. Lett. 118, 042501 (2017), URL https://link.aps. org/doi/10.1103/PhysRevLett.118.042501.
- [17] R. Elwell, C. Schneider, J. Jeet, J. E. S. Terhune, H. W. T. Morgan, A. N. Alexandrova, H. B. Tran Tan, A. Derevianko, and E. R. Hudson, Phys. Rev. Lett. 133, 013201 (2024), URL https://link.aps.org/doi/ 10.1103/PhysRevLett.133.013201.
- [18] C. Zhang, T. Ooi, J. S. Higgins, J. F. Doyle, L. von der Wense, K. Beeks, A. Leitner, G. Kazakov, P. Li, P. G. Thirolf, et al. (2024), arXiv:2406.18719v1 [physics.atom-ph].
- [19] A. M. Dykhne and E. V. Tkalya, JETP Lett. 67, 251 (1998).
- [20] E. V. Tkalya, C. Schneider, J. Jeet, and E. R. Hudson, Phys. Rev. C 92, 054324 (2015), URL https://link. aps.org/doi/10.1103/PhysRevC.92.054324.
- [21] G. Alaga, K. Alder, A. Bohr, and B. Mottelson, Kgl. Danske Videnskab. Selskab Mat.-fys. Medd. 29 (No. 9), 1 (1955).
- [22] S. G. Nilsson, Kgl. Danske Videnskab. Selskab Mat.-fys. Medd. 29 (No. 16), 1 (1955).
- [23] K. Gulda, W. Kurcewicz, A. Aas, M. Borge, D. Burke, B. Fogelberg, I. Grant, E. Hagebø, N. Kaffrell, J. Kvasil, et al., Nuclear Physics A 703, 45 (2002), ISSN 0375-9474, URL http://www.sciencedirect.com/science/ article/pii/S0375947401014567.
- [24] E. Ruchowska, W. A. Płóciennik, J. Żylicz, H. Mach, J. Kvasil, A. Algora, N. Amzal, T. Bäck, M. G. Borge, R. Boutami, et al., Phys. Rev. C 73, 044326 (2006).
- [25] V. G. Soloviev, Theory of Complex Nuclei (Pergamon Press, Oxford, 1976).
- [26] X.-T. He and Z.-Z. Ren, J. Phys. G: Nucl. Part. Phys. 34, 1611 (2007).
- [27] X.-T. He and Z.-Z. Ren, Nucl. Phys. A 806, 117 (2008).
- [28] E. Litvinova, H. Feldmeier, J. Dobaczewski, and V. Flambaum, Phys. Rev. C 79, 064303 (2009).
- [29] N. Minkov and A. Pálffy, Phys. Rev. Lett. 118, 212501 (2017).
- [30] N. Minkov and A. Pálffy, Phys. Rev. Lett. 122, 162502 (2019).
- [31] N. Minkov and A. Pálffy, Phys. Rev. C 103, 014313 (2021).
- [32] S. G. Nilsson and I. Ragnarsson, Shapes and Shells in Nuclear Structure (Cambridge University Press, Cambridge, 1995).
- [33] N. Minkov, P. Yotov, S. Drenska, W. Scheid, D. Bonatsos, D. Lenis, and D. Petrellis, Phys. Rev. C 73, 044315 (2006), URL https://link.aps.org/doi/10.1103/PhysRevC.73.044315.
- [34] N. Minkov, S. Drenska, P. Yotov, S. Lalkovski, D. Bonatsos, and W. Scheid, Phys. Rev. C 76, 034324 (2007), URL https://link.aps.org/doi/10. 1103/PhysRevC.76.034324.
- [35] N. Minkov, Physica Scripta T154, 014017 (2013), URL http://stacks.iop.org/1402-4896/2013/i=T154/a= 014017.
- [36] N. Minkov, S. Drenska, M. Strecker, W. Scheid, and

- H. Lenske, Phys. Rev. C $\bf 85,\,034306$ (2012), URL https://link.aps.org/doi/10.1103/PhysRevC.85.034306.
- [37] N. Minkov, S. Drenska, K. Drumev, M. Strecker, H. Lenske, and W. Scheid, Phys. Rev. C 88, 064310 (2013), URL https://link.aps.org/doi/10. 1103/PhysRevC.88.064310.
- [38] S. Cwiok, J. Dudek, W. Nazarewicz, J. Skalski, and T. Werner, Computer Physics Communications 46, 379 (1987), ISSN 0010-4655, URL http://www.sciencedirect.com/science/article/ pii/0010465587900932.
- [39] L. Bonneau, N. Minkov, D. D. Duc, P. Quentin, and J. Bartel, Phys. Rev. C 91, 054307 (2015).
- [40] M. Beiner, H. Flocard, N. V. Giai, and P. Quentin, Nucl. Phys. A 238, 29 (1975).
- [41] D. Vautherin, Phys. Rev. C 7, 296 (1973).
- [42] L. Bonneau, P. Quentin, N. Minkov, D. Ivanova, J. Bartel, H. Molique, and M.-H. Koh, Bulg. J. Phys. 46, 366 (2019).
- [43] P. Quentin, L. Bonneau, N. Minkov, D. Ivanova, J. Bartel, H. Molique, and M.-H. Koh, Bulg. J. Phys. 48, 634 (2021).
- [44] N. Minkov, L. Bonneau, P. Quentin, J. Bartel, H. Molique, and D. Ivanova, Phys. Rev. C 105, 044329 (2022).
- [45] N. Minkov, L. Bonneau, P. Quentin, J. Bartel, H. Molique, and M.-H. Koh, Phys. Rev. C 109, 064315 (2024), URL https://doi.org/10.1103/PhysRevC.109. 064315.
- [46] J. Dobaczewski, P. Baczyk, P. Becker, M. Bender, K. Bennaceur, J. Bonnard, Y. Gao, A. Idini, M. Konieczka, M. Kortelainen, et al., J. Phys. G: Nucl. Part. Phys. 48, 102001 (2021).
- [47] W. Ryssens, V. Hellemans, M. Bender, and P. H. Heenen, Comp. Phys. Comm. 187, 175 (2015).
- [48] M. Chen, T. Lia, B. Schuetrumpf, P. G. Reinhard, and W. Nazarewicz, Comp. Phys. Comm. 276, 108344 (2022).
- [49] H. Flocard, P. Quentin, A. K. Kerman, and D. Vautherin, Nucl. Phys. A 203, 433 (1973).
- [50] N. Pillet, P. Quentin, and J. Libert, Nucl. Phys. A 697, 141 (2002).
- [51] P. Bonche, H. Flocard, P.-H. Heenen, S. J. Krieger, and M. S. Weiss, Nucl. Phys. A 443, 39 (1985).
- [52] N. M. Nor, N.-A. Rezle, K.-W. Kelvin-Lee, M.-H. Koh, L. Bonneau, and P. Quentin, Phys. Rev. C 99, 064306 (2019).
- [53] D. R. Inglis, Phys. Rev. 96, 1059 (1954), URL https: //link.aps.org/doi/10.1103/PhysRev.96.1059.
- [54] D. R. Inglis, Phys. Rev. 97, 701 (1955), URL https://link.aps.org/doi/10.1103/PhysRev.97.701.
- [55] S. T. Belyaev, Nucl. Phys. 24, 322 (1961).
- [56] E. K. Yuldashbaeva, J. Libert, P. Quentin, and M. Girod, Phys. Lett. B 461, 1 (1999).
- [57] J. Libert, M. Girod, and J. P. Delaroche, Phys. Rev. C 60, 054301 (1999).
- [58] http://www.nndc.bnl.gov/ensdf/.
- [59] K. Nomura, D. Vretenar, T. Nikšić, and B.-N. Lu, Phys. Rev. C 89, 024312 (2014), URL https://link.aps.org/doi/10.1103/PhysRevC.89.024312.
- [60] C. Gustafsson, P. Möller, and S. G. Nilsson, Phys. Lett. B 34, 349 (1971).
- [61] S. A. E. Johansson, Nucl. Phys. 22, 529 (1961).
- [62] S. Ban, J. Dobaczewski, J. Engel, and A. Shukla, Phys.

- Rev. C 82, 015501 (2010).
- [63] A. V. Afanasjev and O. Abdurazakov, Phys. Rev. C 88, 014320 (2013).
- [64] M. S. Safronova, U. I. Safronova, A. G. Radnaev, C. J. Campbell, and A. Kuzmich, Phys. Rev. A 88, 060501(R) (2013), URL https://link.aps.org/doi/ 10.1103/PhysRevA.88.060501.
- [65] S. Gerstenkorn, P. Luc, J. Verges, D. W. Englekemeir, J. E. Gindler, and F. S. Tomkins, J. Phys. (Paris) 35, 483 (1974).
- [66] J. Thielking, M. V. Okhapkin, P. Glowacki, D. M. Meier, L. von der Wense, B. Seiferle, C. E. Düllmann, P. G. Thirolf, and P. Peik, Nature (London) 556, 321 (2018).
- [67] R. A. Müller, A. V. Maiorova, S. Fritzsche, A. V. Volotka, R. Beerwerth, P. Glowacki, J. Thielking, D.-M. Meier, M. Okhapkin, E. Peik, et al., Phys. Rev. A 98, 020503(R) (2018), URL https://link.aps.org/doi/10.1103/PhysRevA.98.020503.
- [68] T. V. N. Hao, P. Quentin, and L. Bonneau, Phys. Rev. C 86, 064307 (2012), URL https://link.aps.org/doi/ 10.1103/PhysRevC.86.064307.
- [69] D. Bonatsos, D. Lenis, N. Minkov, D. Petrellis, and P. Yotov, Phys. Rev. C 71, 064309 (2005).
- [70] W. Nazarewicz, P. Olanders, I. Ragnarsson, G. A. L. J. Dudek, P. Möller, and E. Ruchowska, Nucl. Phys. A 429, 269 (1984).
- [71] D. G. Roux, R. A. Bark, E. A. Lawrie, et al., Eur. Phys. J. A 60, 118 (2024), URL https://doi.org/10.1140/ epja/s10050-024-01337-z.
- [72] P. A. Butler and W. Nazarewicz, Rev. Mod. Phys. 68, 349 (1996).
- [73] P. A. Butler, J. Phys. G: Nucl. Part. Phys. 43, 073002 (2016).
- [74] N. J. Stone, At. Data Nucl. Data Tables 90, 75–176 (2005).
- [75] R. R. Chasman, I. Ahmad, A. M. Friedman, and J. R. Erskine, Rev. Mod. Phys. 49, 833 (1977), URL https://link.aps.org/doi/10.1103/RevModPhys.49.833.
- [76] J. Engel, D. Brink, K. Goeke, S. J. Krieger, and D. Vautherin, Nucl. Phys. A 249, 215 (1975).
- [77] V. Hellemans, P.-H. Heenen, and M. Bender, Phys. Rev. C 85, 014326 (2012).
- [78] P. Ring and P. Schuck, The Nuclear Many-Body Problem (Springer Verlag, New York, 1980).
- [79] M. Chen, T. Li, J. Dobaczewski, and W. Nazarewicz, Phys. Rev. C 103, 034303 (2021).
- [80] K. Nomura, L. Lotina, T. Nikšić, and D. Vretenar, Phys. Rev. C 103, 054301 (2021).
- [81] S. B. Dutta et al., Z. Phys. A **341**, 39 (1991).
- [82] G. A. Leander and Y. S. Chen, Phys. Rev. C 37, 2744 (1988).